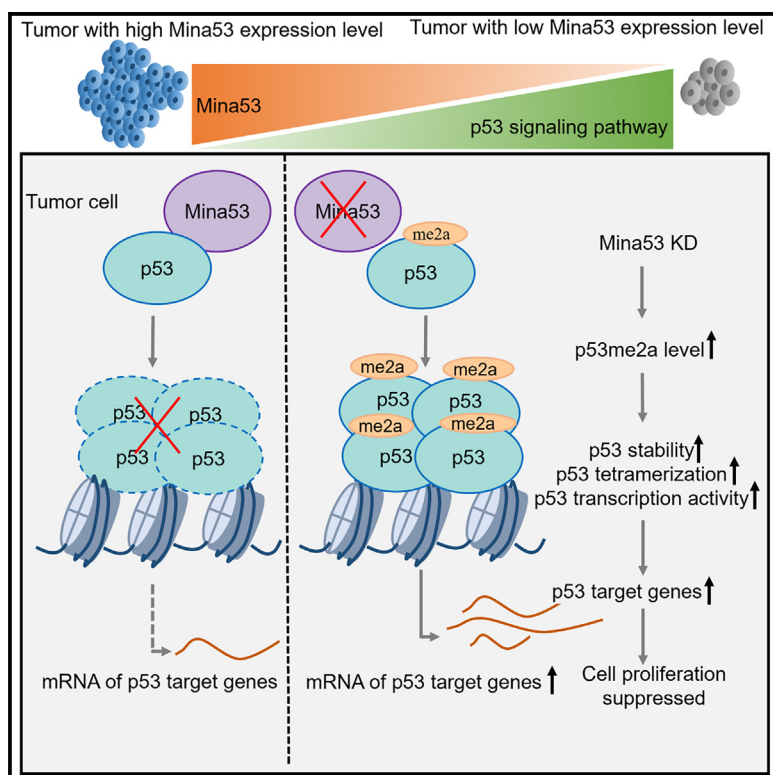


Mina53 catalyzes arginine demethylation of p53 to promote tumor growth

Graphical abstract



Authors

Lixiao Zhou, Liyang Yu, Shushu Song, ..., Chenggang Zhu, Yuanyuan Ruan, Wen Yi

Correspondence

yuanyuanruan@fudan.edu.cn (Y.R.),
wyi@zju.edu.cn (W.Y.)

In brief

Zhou et al. identify an arginine demethylase, Mina53, that catalyzes the removal of Arg337 asymmetric dimethylation of p53, which leads to suppression of p53-mediated signaling to promote tumor growth.

Highlights

- Mina53 negatively regulates p53-mediated cell signaling
- Mina53 is an arginine demethylase to remove Arg337 asymmetric dimethylation of p53
- Mina53-mediated demethylation regulates p53 stability and activity
- Mina53-mediated demethylation is important for tumor growth



Article

Mina53 catalyzes arginine demethylation of p53 to promote tumor growth

Lixiao Zhou,^{1,8} Liyang Yu,^{1,8} Shushu Song,^{2,8} Yong Wang,^{1,3,8} Qiang Zhu,^{1,8} Meng Li,¹ Yutong Sha,¹ Liang Xu,¹ Xin Shu,⁴ Qingqing Liao,⁴ Ting Wu,⁴ Bing Yang,⁴ Siyuan Chai,⁵ Bingyi Lin,⁵ Liming Wu,⁵ Ruhong Zhou,^{1,3,6} Xiaotao Duan,⁷ Chenggang Zhu,¹ Yuanyuan Ruan,^{2,*} and Wen Yi^{1,5,6,9,*}

¹Ministry of Education Key Laboratory of Biosystems Homeostasis & Protection, College of Life Sciences, Zhejiang University, Hangzhou, China

²NHC Key Laboratory of Glycoconjugates Research, Department of Biochemistry and Molecular Biology, School of Basic Medical Sciences, Fudan University, Shanghai, China

³The Provincial International Science and Technology Cooperation Base on Engineering Biology, International Campus of Zhejiang University, Haining, China

⁴Life Science Institute, Zhejiang University, Hangzhou, China

⁵Department of Hepatobiliary and Pancreatic Surgery, The First Affiliated Hospital, Zhejiang Provincial Key Laboratory of Pancreatic Disease, School of Medicine, Zhejiang University, Hangzhou, China

⁶Cancer Center, Zhejiang University, Hangzhou, China

⁷State Key Laboratory of Toxicology and Medical Countermeasures, Beijing Institute of Pharmacology and Toxicology, Beijing, China

⁸These authors contributed equally

⁹Lead contact

*Correspondence: yuanyuanruan@fudan.edu.cn (Y.R.), wyi@zju.edu.cn (W.Y.)

<https://doi.org/10.1016/j.celrep.2025.115242>

SUMMARY

Arginine methylation is a common post-translational modification that plays critical roles in many biological processes. However, the existence of arginine demethylases that remove the modification has not been fully established. Here, we report that Myc-induced nuclear antigen 53 (Mina53), a member of the jumonji C (JmjC) protein family, is an arginine demethylase. Mina53 catalyzes the removal of asymmetric dimethylation at arginine 337 of p53. Mina53-mediated demethylation reduces p53 stability and oligomerization and alters chromatin modifications at the gene promoter, thereby suppressing p53-mediated transcriptional activation and cell-cycle arrest. Mina53 represses p53-dependent tumor suppression both in mouse xenografts and spontaneous tumor models. Moreover, downregulation of p53-mediated gene expression is observed in several types of cancer with elevated expression of Mina53. Thus, our study reveals a regulatory mechanism of p53 homeostasis and activity and, more broadly, defines a paradigm for dynamic arginine methylation in controlling important biological functions.

INTRODUCTION

Arginine methylation is a common post-translational modification of eukaryotic proteins. Studies have demonstrated the critical role of arginine methylation in regulating various biological processes, including gene transcription, RNA biogenesis, metabolic regulation, and signal transduction.^{1–5} To date, at least nine protein arginine methyltransferases (PRMTs), which are classified into three subtypes, have been identified to transfer the methyl group from S-adenosylmethionine to the arginine residues of proteins.² Extensive research efforts on PRMTs and their relevance in diseases have led to significant progress in the development of therapeutic strategies targeting these enzymes.^{2,5} Arginine methylation is known to be a dynamic process in cells.^{6–9} However, in contrast to the progress made in arginine methylation, the study of arginine demethylation has lagged largely behind. The identification and characterization of *bona fide* arginine demethylases is crucial for unraveling

the functional significance of dynamic arginine methylation in biological processes.

TP53 (p53) is a well-known transcription factor that regulates a number of essential biological processes, including the cell cycle, apoptosis, and metabolism.^{10,11} Its activity in cells is tightly regulated at both the transcriptional and translational levels. Studies have revealed a variety of post-translational modifications on p53 that contribute to its cellular homeostasis and activation in response to stress.^{12–15} For example, phosphorylation at the amino terminus of p53 regulates its degradation via the ubiquitin-mediated pathway.^{15,16} Acetylation of lysine residues at various sites has been shown to affect p53's DNA-binding activity and its interaction with other transcription factors.^{14,17–19} Moreover, p53 is extensively modified by lysine methylation, which regulates p53 function in both positive and negative manners depending on the sites of modification.^{19–23} More recently, p53 has been reported to contain arginine methylation at the C-terminal region.^{24,25} Arginine methylation has been found to



promote p53 nuclear localization and oligomerization, thus positively regulating its function in response to stress signals. Collectively, these reports suggest a complex regulatory mechanism for p53 homeostasis and function that remains far from being completely understood.

Myc-induced nuclear antigen 53 (Mina53; also termed RIOX2) is a direct *c-myc* target gene product and belongs to the jumonji C (JmjC) domain-containing protein family. Previous studies suggested a dual role of Mina53: lysine demethylase activity toward histone H3 lysine 9 trimethylation and hydroxylase activity toward the ribosomal protein L27A.^{26–28} Mina53 expression is frequently elevated in different types of human cancers, including colon cancer, lung cancer, renal cancer, and leukemia.^{29–32} High levels of Mina53 expression have been shown to correlate with poor prognosis and survival in patients.^{30,31} However, the exact molecular function of Mina53 still remains elusive, and how Mina53 contributes to cancer development is largely unknown.

Here, we identified an enzymatic activity of Mina53 as the arginine demethylase. Mina53 catalyzes removal of the asymmetric dimethylation from R337 of p53, which results in decreased p53 oligomerization, reduced binding of p53 to target gene promoters, and enhanced p53 ubiquitination and degradation and ultimately leads to reduced p300-dependent histone acetylation at the promoters of p53 target genes. Thus, Mina53 acts as a co-repressor of p53 signaling in cells. Our findings reveal an additional level of complexity in the regulation of p53 homeostasis and, more broadly, establish arginine demethylation as a key mechanism in controlling biological functions.

RESULTS

Mina53 represses p53-mediated cell signaling

To investigate the function of Mina53 in tumor development, we first analyzed RNA sequencing data from The Cancer Genome Atlas (TCGA). Gene set enrichment analysis (GSEA) revealed a significant negative enrichment of p53-inducible targets in colon cancer samples with high *Mina53* expression (Figure 1A). Similarly, a reverse correlation between *Mina53* expression and p53-inducible targets was also observed in lung squamous cell carcinoma and gastric cancer (Figures S1A and S1B). Hence, *Mina53* expression was negatively correlated to the expression of p53-regulated genes in these cancers. Interestingly, no significant correlation was found between *Mina53* expression and the mutational status of *p53* in colon cancer (Figure S1C). To corroborate the database analysis, we obtained 50 colorectal tumor samples with wild-type *TP53*, as determined by exon sequencing, and assessed the correlation between *Mina53* expression and p53 target genes (Table S1). As expected, the expression of *Mina53* was inversely correlated with the expression of the p53 target genes *p21* and *Fas* (Figure 1B). Furthermore, tissue microarray analysis of an additional cohort of 58 pairs of tissue samples showed higher protein expression of Mina53 in tumor tissues compared to adjacent normal tissues (Figures S1C–S1E; Table S2). Thus, these results suggest that Mina53 inhibited p53-mediated function.

We next investigated the role of Mina53 in p53-mediated transcriptional regulation in cultured cell lines. Knockdown of Mina53

using *Mina53*-targeting short hairpin RNA (shRNA) significantly increased both the protein level and mRNA level of *p21* in colon cancer HCT116 cells (Figures 1C and 1D). Notably, knockdown of Mina53 was associated with a significant increase in p53 protein expression. Similar results were observed in breast cancer MCF-7 cells and lung cancer A549 cells (Figures S1F and S1G). To determine whether the elevated *p21* expression upon Mina53 knockdown was dependent on *p53*, we used isogenic HCT116 *p53*^{−/−} cells. The increased *p21* expression was abolished in HCT116 *p53*^{−/−} cells upon Mina53 knockdown (Figures 1C and 1D). A similar observation was shown in lung cancer H1299 cells that are *p53* null (Figure S1H). Furthermore, transcriptome analysis showed that *p53* target genes were upregulated upon Mina53 knockdown in HCT116 cells (Figures 1E and 1F; Table S3). This effect was diminished in HCT116 *p53*^{−/−} cells (Figure 1F). Chromatin immunoprecipitation (ChIP) assays revealed that, upon Mina53 knockdown, *p53* was enriched at the promoters of *p21* and *TIGAR*, even after normalization of *p53* protein levels (Figures 1G and S1I). As Mina53 is a direct transcriptional target of c-Myc, we confirmed that depletion of c-Myc reduced Mina53 expression while concomitantly increasing *p53* and *p21* expression (Figure 1J). Together, these results demonstrated that Mina53 represses *p53*-mediated transcriptional activation.

Upon DNA damage, *p53* induces cell-cycle arrest and apoptosis.^{33,34} Depletion of Mina53 in HCT116 cells caused G1 phase cell-cycle arrest compared to control cells (Figure 1H). In contrast, in HCT116 *p53*^{−/−} cells, the cell-cycle arrest effect was largely diminished (Figure 1H). Additionally, Mina53 depletion in HCT116 cells resulted in a higher percentage of apoptotic cells (Figure 1I). In the presence of doxorubicin (Dox), the apoptotic population increased even further upon Mina53 knockdown. Consistently, the effect on apoptosis was largely abolished in HCT116 *p53*^{−/−} cells (Figure 1I). Together, these results suggest that Mina53 represses *p53*-dependent cell-cycle arrest and apoptosis.

Mina53 interacts with p53 in cells

To further investigate the mechanism by which Mina53 negatively regulates p53-mediated signaling, we assessed whether *p53* interacts with Mina53. Co-immunoprecipitation (coIP) assays revealed the association between endogenous *p53* and Mina53 in both HCT116 and A549 cells (Figure 2A). This interaction was also confirmed in HEK293T cells with ectopic expression of epitope-tagged *p53* and Mina53 followed by coIP (Figure 2B). Additionally, a direct interaction was demonstrated using bacterially purified proteins (Figure 2C). Thus, *p53* directly interacts with Mina53 in cells.

The interaction between *p53* and Mina53 was significantly reduced following treatment with Dox to induce DNA damage (Figure 2D). Dox treatment also induced phosphorylation of *p53* on S15 (Figure S2A).^{35,36} To investigate whether decreased interaction is due to phosphorylation, we co-expressed hemagglutinin (HA)-tagged Mina53 and FLAG-tagged wild-type (WT), S15A, or S15D *p53* in HEK293T cells and performed coIP assays.

We observed that S15A and S15D *p53* pulled down similar amounts of Mina53 compared to WT *p53* (Figure 2B).

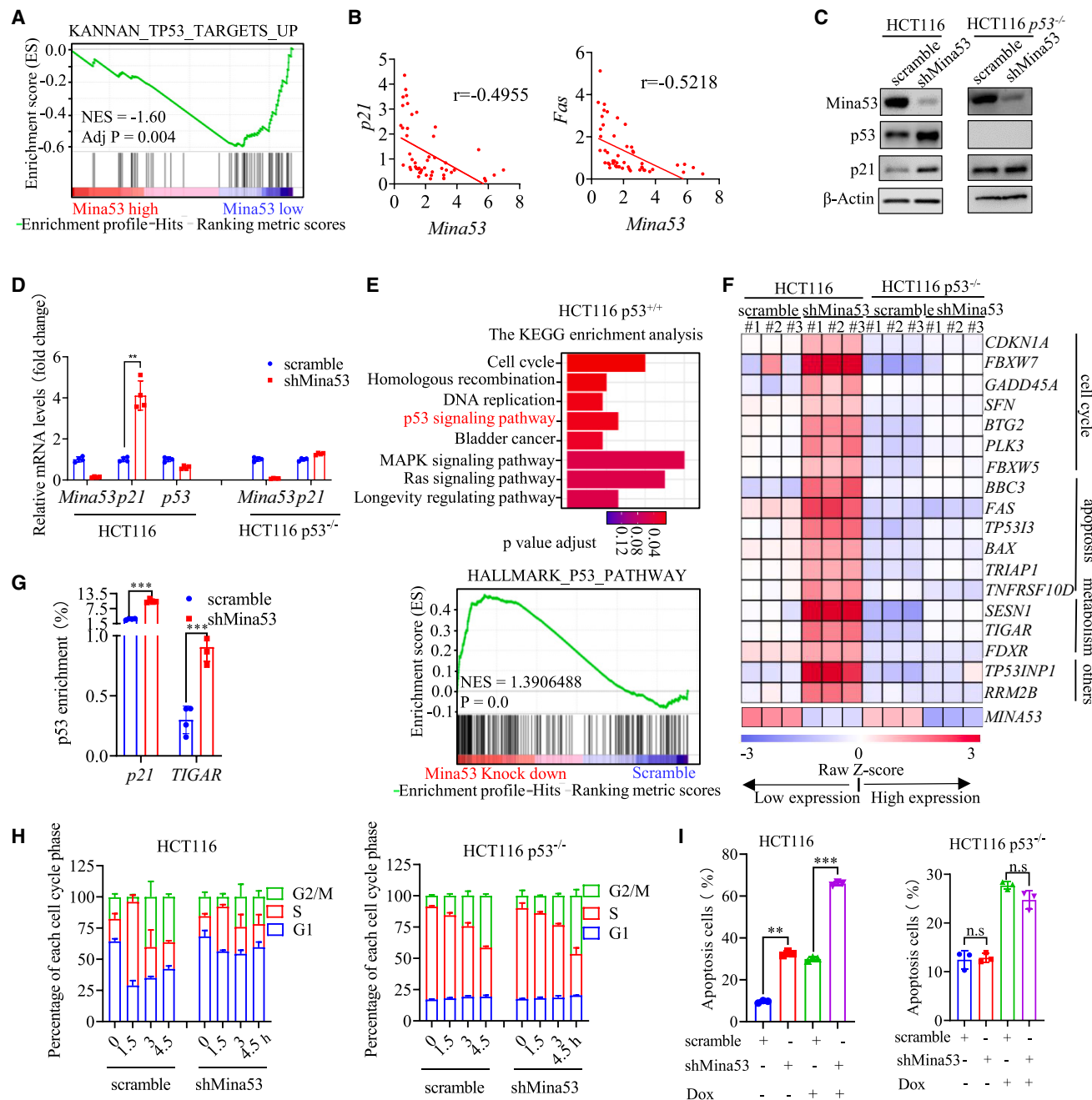


Figure 1. Mina53 negatively regulates p53-mediated signaling

- (A) GSEA to evaluate changes in the gene signature of the p53-mediated pathway in colon cancer samples with high *Mina53* expression from the TCGA database.
- (B) The correlation of the mRNA expression levels of *Mina53* vs. *p21* or *Fas* from 50 clinical colon cancer samples containing WT *TP53*.
- (C) Immunoblot analysis of p53 and p21 expression in HCT116 and HCT116 $p53^{-/-}$ cells upon Mina53 shRNA lentiviral transduction.
- (D) Relative *p21* mRNA level in HCT116 cells and HCT116 $p53^{-/-}$ cells upon Mina53 knockdown.
- (E) The Kyoto Encyclopedia of Genes and Genomes (KEGG) pathway analysis (top) of HCT116 cells and HCT116 $p53^{-/-}$ cells transduced with lentiviruses carrying Mina53 shRNA or scramble shRNA. GSEA (bottom) was used to evaluate changes in the gene signature of the p53-mediated pathway.
- (F) Heatmap of the changes of p53 target genes upon depletion of *Mina53* in HCT116 and HCT116 $p53^{-/-}$ cells.
- (G) The enrichment of p53 to the target gene promoters upon Mina53 knockdown in HCT116 cells with normalization to the p53 level.
- (H) Analysis of the cell cycle progression in HCT116 and HCT116 $p53^{-/-}$ cells upon Mina53 shRNA lentiviral transduction.
- (I) Analysis of the apoptosis of HCT116 and HCT116 $p53^{-/-}$ cells upon Mina53 shRNA lentiviral transduction after treatment with Dox for 12 h.
- Error bars denote the mean \pm SD; $n = 3$ assays. Statistical analyses were performed by unpaired two-tailed Student's t test (* $p < 0.05$, ** $p < 0.01$, *** $p < 0.001$).

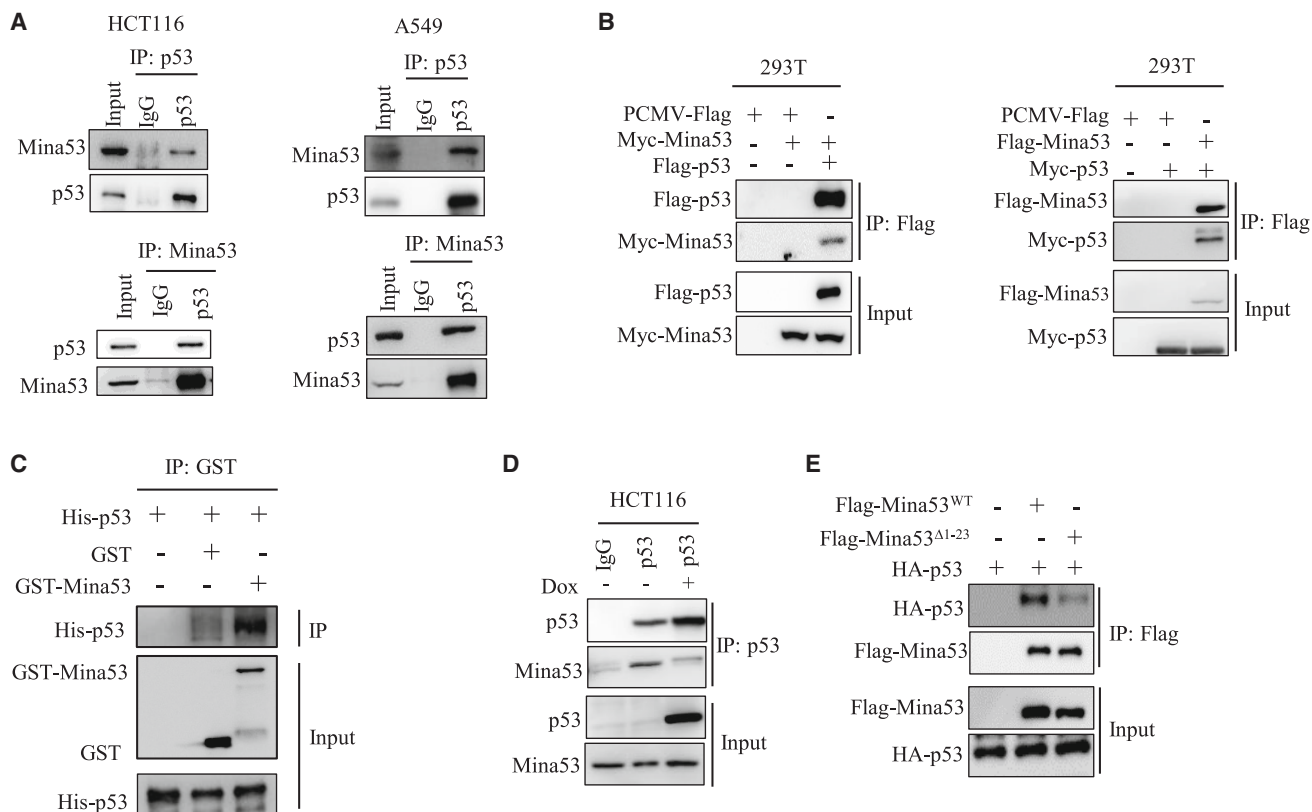


Figure 2. Mina53 interacts with p53

(A) Immunoblot analysis of the endogenous interaction between p53 and Mina53 in HCT116 cells or A549 cells.
 (B) Immunoblot analysis of the interaction between epitope-tagged p53 and Mina53 co-expressed in HEK293T cells. The protein complex was immunoprecipitated using FLAG-M2 beads and detected by the indicated antibody.
 (C) Immunoblot analysis of the interaction between purified, bacterially expressed, His-tagged p53 and glutathione S-transferase (GST)-tagged Mina53.
 (D) Immunoblot analysis of the endogenous interaction between Mina53 and p53 upon Dox treatment in HCT116 cells.
 (E) Immunoblot analysis of the interaction between epitope-tagged full length or N terminus-truncated Mina53 and p53 co-expressed in HEK293T cells. The protein complex was immunoprecipitated using FLAG-M2 beads and detected by an HA antibody.

Error bars denote the mean \pm SD; $n = 3$ assays. Statistical analyses were performed by unpaired two-tailed Student's t test (* $p < 0.05$, ** $p < 0.01$, *** $p < 0.001$).

Additionally, we performed pull-down experiments using p53 S9A and S20A with Mina53, as both S9 and S20 have been reported as phosphorylation sites.^{37,38} These p53 mutants also pulled down similar amounts of Mina53 as compared to the WT p53 (Figure S2B). Together, these results suggest that phosphorylation of p53 at its N terminus had no effect on p53-Mina53 interaction.

To determine the binding region of Mina53 with p53, we performed chemical cross-linking of the purified proteins followed by mass spectrometry. The result mapped the binding region to the N terminus of Mina53 and the C terminus of p53 (Figure S2C). Consistently, truncation of 23 amino acid from the N terminus of Mina53 (termed Mina53^{Δ1–23}) led to a marked reduction in its interaction with p53, supporting the theory that the N terminus of Mina53 is critical for Mina53-p53 interaction (Figure 2E). Notably, ectopic expression of Mina53^{Δ1–23} in cells had only a slight effect on p53 protein level and *p21* mRNA level, in contrast to the drastic effect seen with WT Mina53 expression (Figures S2D and S2E). In addition, ChIP assays showed that the enrichment of p53 at the *p21* gene promoter was decreased

upon expression of WT Mina53, but not Mina53^{Δ1–23}, compared to the control group (Figure S2F). Together, these data emphasize the critical role of Mina53-p53 interaction in p53 function.

Mina53 catalyzes arginine demethylation on p53

Mina53 is a member of the JmJc domain-containing protein family, which includes proteins with lysine and/or arginine demethylase activities.^{39–41} A previous study demonstrated that p53 lysine demethylation is catalyzed by LSD1.¹³ We observed that depletion of Mina53 did not affect p53 lysine methylation but, rather, impacted p53 arginine methylation, as detected using pan-antibodies (Figure S3A). To further exclude the impact of Mina53 knockdown-induced upregulation of the p53 protein level, we treated HCT116 cells with Dox and measured the R337me2a level. Compared to the control group, Mina53 depletion resulted in increased p53R337me2a levels (Figure S3A). Arginine methylation has been reported at residues arginine 333 (R333, mono-methylation) and R335 and R337 (both dimethylation) in p53.²⁵ Consistently, we confirmed the presence of dimethylation on these residues on endogenous p53 using

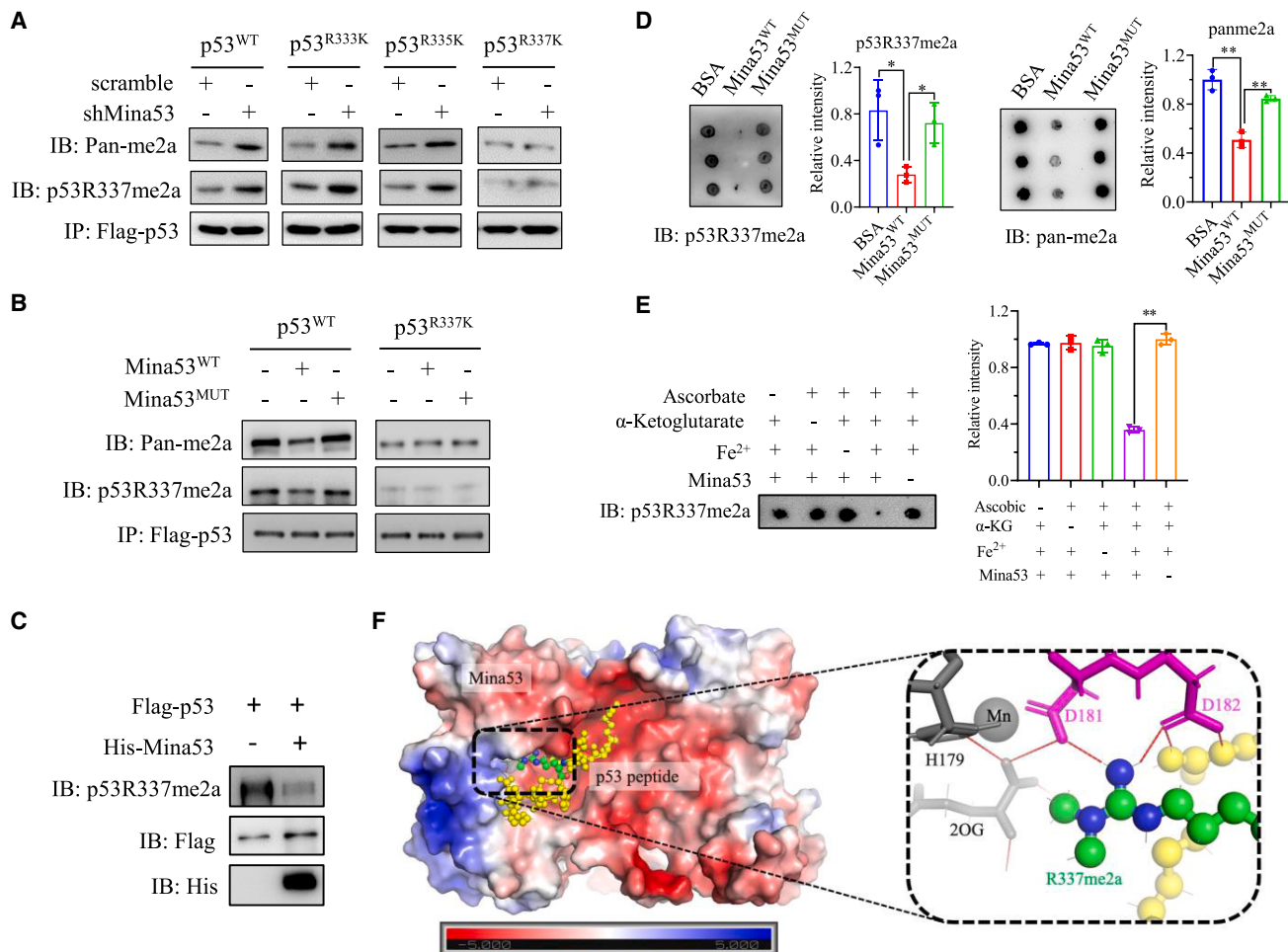


Figure 3. Mina53 catalyzes the removal of p53 R337 asymmetric dimethylation

(A and B) Immunoblot analysis of p53 R337 asymmetric dimethylation upon Mina53 knockdown (A) and ectopic expression of WT or inactive mutant Mina53 (B) in HCT116 cells. Samples were adjusted for equal loading of p53 to facilitate comparison.

(C and D) Dot-blot analysis of Mina53-mediated demethylation reactions using synthetic p53R337me2a peptide in normal demethylation assay buffer (C) or with various reaction components (D). The bar graph represents quantification of blotting signal intensity.

(E) Immunoblot analysis of R337me2a signal of FLAG-tagged p53 in the presence or absence of bacterially purified His-tagged Mina53 in the *in vitro* reaction. (F) Interactions between Mina53 and a peptide containing p53R337me2a, revealed by molecular docking and MD simulation.

Error bars denote the mean \pm SD; $n = 3$ assays. Statistical analyses were performed by unpaired two-tailed Student's t test (* $p < 0.05$, ** $p < 0.01$, *** $p < 0.001$).

mass spectrometry (Figure S3B). As arginine dimethylation exists in both asymmetric and symmetric forms, we next investigated the specific forms of dimethylation on R335 and R337 using pan-antibodies against arginine asymmetric or symmetric dimethylation, respectively. Western blot results indicated that R335 is a major site for symmetric dimethylation (me2s) and that R337 is predominantly modified by asymmetric dimethylation (me2a; Figure S3C). Upon Mina53 knockdown, we observed increased asymmetric dimethylation on p53, an effect that was abolished on the R337K mutant but not in R333K or R335K mutants, suggesting that Mina53 may catalyze the removal of R337me2a (Figure 3A). The result was further confirmed with a customized site-specific p53 antibody against R337me2a (Figures 3A and S3D). In addition, ectopic expression of WT Mina53, but not the catalytically inactive mutant (H179Y/

D181G/H240Y),²⁶ reduced R337 methylation in cells with no effect on the R337K mutant (Figure 3B). These results suggest that Mina53 mediates the removal of R337me2a on p53. To investigate this further, we selected several well-characterized demethylases from the JmjC family and individually knocked down these proteins in cells (Figures 3E–3I). Depletion of individual proteins did not lead to increased p53 protein expression or *p21* mRNA expression (Figures 3E–3I). Notably, only depletion of Mina53, but not others, led to a significant increase in R337 methylation (Figure 3J), indicating that the effect on p53 R337 methylation was specifically mediated by Mina53.

To further characterize the demethylation activity of Mina53, we bacterially expressed and purified the His-tagged WT or an inactive mutant of Mina53 and performed *in vitro* demethylation reactions with synthetic methylated peptides. The reactions

were analyzed with a dot-blot assay and a formaldehyde generation assay (Figures 3C and S3K; peptide sequences can be found in the supplemental information). Both assays consistently demonstrated robust demethylation activity of Mina53. As expected for a typical demethylation reaction, omission of any key reaction components significantly impaired Mina53 activity (Figure 3D). High-resolution mass spectrometry analysis revealed that incubation of the R337me2a peptide with the WT but not the inactive mutant Mina53 resulted in peaks that were shifted 14 Da from the original substrate peak, corresponding to the molecular ions of the mono-methylated peptide (Figure S4A). Incubation of R337me1 peptide in the reaction led to a very modest appearance of peaks consistent with the molecular ions of the non-methylated peptide (Figure S4B). To further confirm the arginine demethylase activity of Mina53 toward p53 protein, we established HEK293T cells stably expressing PRMT6 and FLAG-tagged p53. Purified p53 was then incubated with His-tagged Mina53, which was purified from *E. coli*, in demethylation assay buffer, followed by mass spectrometry analysis. We observed the loss of the chromatographic peak corresponding to R337me2a in the tryptically digested peptide in the Mina53-containing reaction but not in the control reaction (Figures S4C and S4D). Consistently, His-tagged Mina53 catalyzed the removal of R337me2a from FLAG-tagged p53, as analyzed by immunoblotting (Figure 3E). This result strongly supports the demethylation activity of Mina53 toward p53. Incubation with other forms of methylated peptides did not yield any detectable products (Figures S5A–S5E), further confirming the specificity of Mina53. The enzyme kinetics study showed that Mina53 had a K_m value of 1.64 μM and a turn-over rate (kcat) of 0.157 s^{-1} for the R337me2a peptide substrate. Collectively, the cellular and biochemical data demonstrate that Mina53 is an arginine demethylase that catalyzes demethylation of R337me2a on p53.

We next investigated the structural basis of Mina53-mediated demethylation. Initial attempts to obtain protein-substrate complexes via co-crystallization were unsuccessful. We then turned to molecular docking and explicit-solvent all-atom molecular dynamics (MD) simulation to explore the interaction between Mina53 and the p53 substrate peptide (333-RGRER_{me2a}FEMFR-342). The docked Mina53-peptide complex was stable during a 500 ns MD simulation (Video S1). It revealed that the substrate peptide binds to a negatively charged surface of Mina53 formed between its N- and C-terminal domains. The side chain of R337me2a is positioned deep within the pocket and forming well-defined, catalytically important salt bridges and hydrogen bonds with the surrounding residues His179, Asp181, and Asp182 and the substrate 2-oxoglutarate (2OG) (Figure 3F). To further validate the MD simulation result, we used the docking information to perform disulfide bond crosslinking to obtain protein-substrate complexes. The model predicted the close proximity of Y209 of Mina53 to G334 of the peptide substrate. Thus, these two residues were individually mutated to cysteines to enable specific disulfide bond formation, which was subsequently confirmed by mass spectrometry (Figures S5F and S5G). Together, the structural modeling and crosslinking experiment support the identification of Mina53 as an arginine demethylase.

Asymmetric dimethylation on R337 is critical for p53-mediated signaling

Next, we investigated the role of R337me2a in p53-mediated signaling. We used a small molecule inhibitor (MS023) to suppress the activity of type I protein arginine methyltransferases, which are known to catalyze arginine asymmetric dimethylation.^{42,43} Treatment with MS023 significantly reduced p53 methylation, as detected by the pan-antibody against me2a or with the site-specific antibody against p53R337me2a (Figure 4A). Ectopic expression of WT or R337K p53 in HEK293T cells followed by treatment with increasing concentrations of MS023 showed a clear decrease of arginine methylation of the WT but not R337K p53 (Figure 4B), thus further confirming the presence of asymmetric dimethylation on R337 of p53.

Treatment of HCT116 cells with increasing concentrations of MS023 for 24 h reduced p53 protein levels in a dose-dependent manner without affecting mRNA levels (Figures 4C and 4D). The mRNA level of p21 was consistently decreased (Figure 4D). p53 protein levels were reduced in both the nucleus and cytoplasm (Figure S6A). Furthermore, MS203 treatment decreased the protein expression of WT but not R337K p53 in reconstituted HCT116 p53^{-/-} cells (Figure 4E). When cells were treated with cycloheximide (CHX) to inhibit new protein synthesis, p53 showed a faster degradation rate with MS203 treatment compared to the control with DMSO (Figure 4F). Consistently, WT p53 degraded more rapidly than R337K p53 in the presence of MS023 (Figure S6B). Together, these results suggest that R337me2a promotes p53 protein stability.

Residue R337 is located in the oligomerization domain of p53.⁴⁴ To investigate whether R337me2a is important for p53 oligomerization, we ectopically expressed WT, R335K, R337K, R337H, and 2RK (doublet mutant) p53 in HEK293T cells and analyzed the oligomerization status of these p53 variants. The p53 variants containing the R337 mutation (R337K, R337H, and 2RK) exhibited reduced oligomerization (Figure 4G). Treatment with MS023 reduced the oligomerization of WT p53 to a level comparable to that of R337K p53 (Figure 4H). To further investigate the impact of R337me2a on p53 oligomerization, we performed *in silico* all-atom MD simulations of tetrameric p53 containing R337me2a. The simulations revealed that the asymmetrically dimethylated R337 residues remained stably positioned at the interfaces of the p53 tetramer throughout the simulation, contributing substantial interfacial interactions between p53 monomers (Figure S6C; Video S2). Although R337me2a is positively charged, we found that R337me2a formed extensive interactions beyond salt bridges, including hydrophobic (the side-chain guanidinium group interacts with aromatic and aliphatic side chains above and below the guanidinium plane) and hydrogen-bonding interactions, as revealed by the interaction map of the p53 tetramer (Figure S6D). Together, these results suggest that R337me2a promotes p53 oligomerization.

As oligomerization of p53 is crucial for its transcription activity, we performed a ChIP assay and found that R337K reduced the binding of p53 to the promoters of its target genes compared to WT p53 (Figure S6E). Consistently, real-time PCR assays showed that mRNA levels of p21, FAS, and TIGAR were significantly lower in HCT116 p53^{-/-} cells reconstituted with R337K

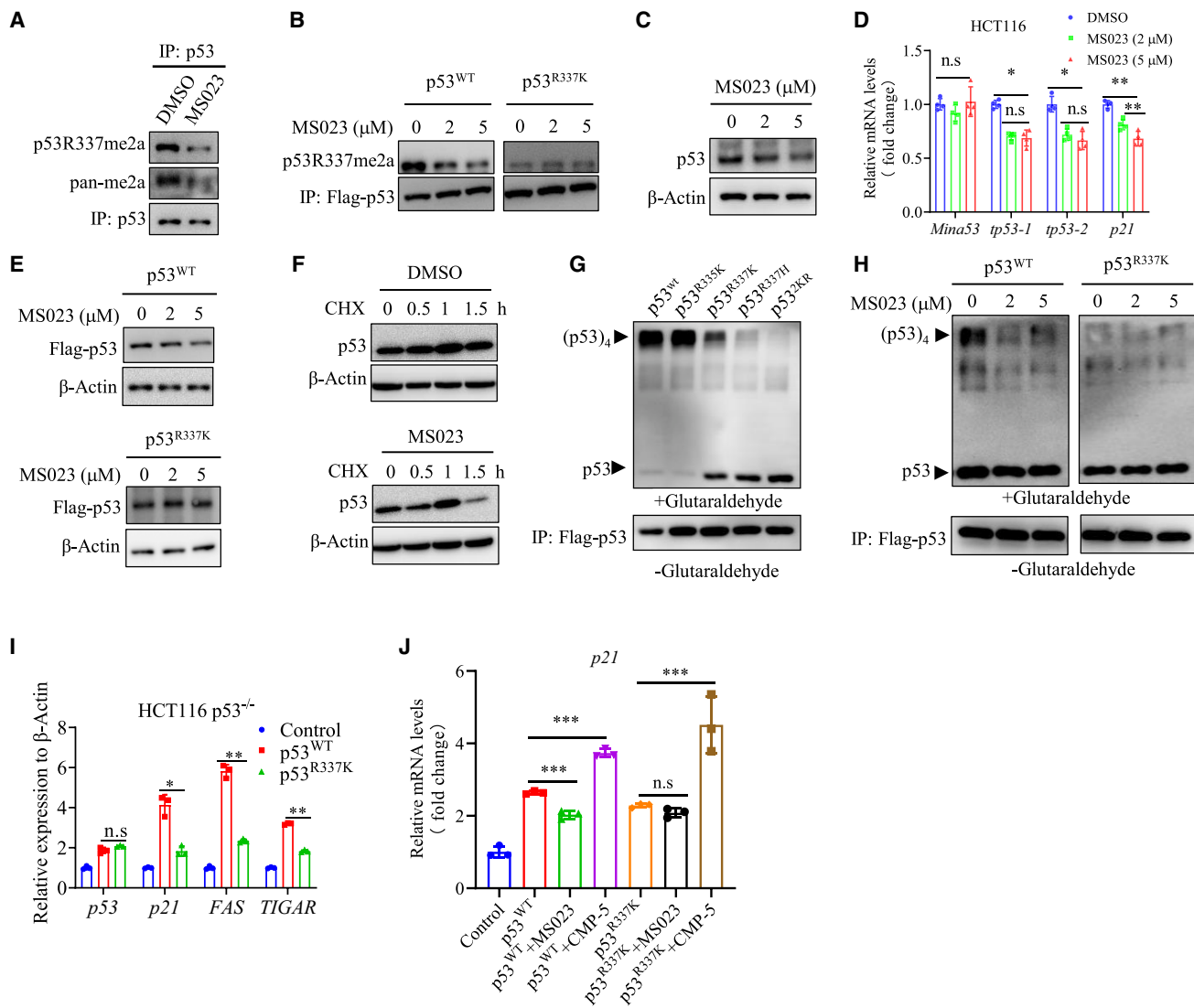


Figure 4. Asymmetric dimethylation on R337 is critical for p53-mediated signaling

- (A) Immunoblot analysis of p53 arginine asymmetric dimethylation in HCT116 cells upon treatment with MS023.
 - (B) Immunoblot analysis of p53 R337me2a in HEK293T cells transfected with FLAG-tagged p53^{WT} or p53^{R337K} in the presence or absence of MS023 at the indicated concentrations for 24 h.
 - (C) Immunoblot analysis of p53 endogenous levels in HCT116 cells in the presence or absence of MS023 at the indicated concentrations for 24 h.
 - (D) The mRNA levels of Mina53, p53, and p21 in HCT116 cells in the presence or absence of MS023 at the indicated concentrations for 24 h.
 - (E) Immunoblot analysis of the expression of FLAG-tagged p53^{WT} or p53^{R337K} in reconstituted HCT116 p53^{-/-} cells in the presence or absence of MS023 at the indicated concentrations.
 - (F) Immunoblot analysis of p53 protein expression in HCT116 cells pre-treated with 2 μ M MS023 for 24 h and in the presence of CHX at the indicated time points.
 - (G and H) Immunoblot analysis of the oligomerization states of WT or various mutants of p53 (G) and the oligomerization states of WT or R337K p53 in the presence or absence of MS023 (H).
 - (I) The mRNA levels of p53 and its target genes in HCT116 p53^{-/-} cells reconstituted with WT or R337K p53.
 - (J) The mRNA levels of p21 in HCT116 p53^{-/-} cells reconstituted with WT or R337K p53 in the presence of MS023 or CMP-5 (a PRMT5 inhibitor).
- Error bars denote the means \pm SD, $n = 3$ assays. Statistical analyses were performed by unpaired two-tailed Student's t-test (* $p < 0.05$, ** $p < 0.01$, *** $p < 0.001$).

than with WT p53 (Figure 4I). Moreover, treatment with MS023 significantly decreased the mRNA level of p21 in WT p53 reconstituted cells but not in R337K p53 reconstituted cells (Figure 4J). In contrast, treatment with the pan-inhibitor CMP-5, which targets symmetric dimethylation, increased the transcription

activity of both WT and R337K p53 (Figure 4J).^{45,46} Thus, these results demonstrate that R337me2a negatively regulates transcriptional activity of p53.

We further analyzed the nuclear localization of p53 following ectopic expression of WT or R337K p53 in HCT116 p53^{-/-} cells.

No significant difference in localization was observed between the two p53 variants (Figure S6F). Similarly, Mina53 depletion had no effect on the subcellular localization of the endogenous p53 (Figure S6G).

Mina53-mediated demethylation regulates p53 transcriptional activity, oligomerization, stability, and chromatin modifications

To further assess whether Mina53-mediated demethylation is required for the repression of p53 transcriptional activity, we ectopically expressed the WT or the inactive mutant of Mina53 along with p53 in HCT116 *p53*^{-/-} cells. The luciferase signal used to measure p53-driven transcriptional activity was reduced in cells expressing WT Mina53 but not the mutant (Figure 5A). Furthermore, Mina53 expression decreased the luciferase signal in the presence of WT but not R337K p53 (Figure 5A). Consistently, the luciferase signal was increased upon Mina53 knockdown in the presence of WT but not R337K p53 (Figure 5B). As expected, Mina53 knockdown also led to an increase in the mRNA levels of *p21* and *TIGAR* in the presence of WT but not R337K p53 (Figure S6H). Both the WT and the inactive mutant Mina53 showed a comparable interaction with WT p53 (Figure S6I). In contrast, R337K p53 showed a reduced interaction with Mina53 compared to WT p53 (Figure S6J). ChIP assays further revealed that ectopic expression of WT Mina53, but not the inactive mutant, reduced the binding of p53 to the *p21* gene promoter after normalizing with the p53 expression level (Figure 5C). Additionally, compared to the WT, R337K p53 showed reduced binding to the gene promoters (Figure S6K). These results collectively indicate that Mina53 represses p53 transcriptional activity through R337 demethylation.

Both the demethylase and hydroxylase activities of Mina53 require Mn²⁺ cations and the substrate 2OG for catalysis. The catalytically inactive mutant Mina53 used here presumably loses both activities. To rule out the possibility that the anti-p53 function of Mina53 is a secondary effect due to its hydroxylase activity, we performed a series of experiments. The N terminus-truncated mutant Mina53 (Mina53^{Δ1-23}) largely lost its interaction with p53 but retained intact hydroxylase activity, as it efficiently catalyzed the hydroxylation of a peptide derived from the known hydroxylation target PRL27 (Figure S7A). His39 was identified as the hydroxylation site.²⁸ Expression of PRL27^{H39F}, in which His39 was mutated to phenylalanine to block hydroxylation, in HCT116 cells had no effect on the mRNA expression of the p53 target genes *p21* and *FAS* (Figure S7B), suggesting that Mina53 hydroxylase activity does not regulate p53 function. Ectopic expression of Mina53^{Δ1-23} in cells had diminished effects on p53, including p53R337me2a levels, p53 protein degradation, p53 target gene expression, and enrichment of p53 on the *p21* gene promoter (Figures S2E, S2F, S7C, and S7D). Additionally, we employed a targeted inhibition strategy. We designed and synthesized a peptide containing the R337me2a modification to competitively inhibit p53 R337me2a without manipulating Mina53. A cell-penetrating peptide sequence was also included to facilitate intracellular delivery of the p53 peptide. We observed a significant increase of p53R337me2a levels in cells treated with the methylated peptide but not the non-methylated peptide, consistent with the inhibition of Mina53 demethylation.

lase activity toward p53 (Figure S7E). Moreover, mRNA levels of p53 target genes, including *p21*, *FAS*, and *NOX*, were upregulated in cells treated with the methylated peptide, consistent with the activation of p53 function (Figure S7F). Taken together, these data further support the theory that the regulation of p53 function is specifically mediated by Mina53-dependent demethylation.

Expression of the WT but not the inactive mutant Mina53 reduced the oligomerization state of p53 (Figure 5D). Consistently, depletion of Mina53 increased p53 oligomerization (Figure S8A), suggesting that Mina53-mediated demethylation regulates p53 oligomerization. Depletion of Mina53 in HCT116 and A549 cells resulted in an increase in p53 protein levels (Figures 1C and S1F). When treated with CHX, p53 exhibited a slower degradation rate in HCT116 and A549 cells expressing Mina53 shRNA compared to cells expressing the control shRNA (Figures 5E and S8B). Consistently, expression of the WT but not the inactive mutant Mina53 significantly reduced p53 stability in HCT116 cells and A549 cells (Figures 5F and S8C). The mRNA level of p53 did not show a significant change under these conditions. In addition, the half-life of WT p53 was longer than that of R337K p53 (Figure S8D). Together, these results suggest that Mina53-mediated demethylation reduces p53 protein stability.

Previous studies have demonstrated that MDM2 functions as the primary E3 ubiquitin ligase to promote p53 degradation.⁴⁷⁻⁴⁹ We verified that depletion of MDM2 markedly increased p53 expression in cells expressing WT or the inactive mutant Mina53 (Figure S8E). Under normal conditions, MDM2 forms a stable interaction with p53 to keep p53 at a low level. Upon stress, the interaction of p53 with MDM2 is largely diminished (Figure S8F).⁴⁷ Notably, upon Mina53 knockdown the interaction of p53 with MDM2 was significantly reduced, with a concomitant reduction in p53 ubiquitination (Figure 5G). Expression of WT but not inactive mutant Mina53 enhanced p53-MDM2 interaction (Figure 5H). Consistently, MDM2 formed a stronger interaction with R337K p53 compared to WT p53, leading to a higher ubiquitination level on R337K p53 (Figures S8G and S8H). To exclude the possibility of a direct effect of Mina53 on MDM2, we performed coIP using an anti-Mina53 antibody and found that Mina53 did not interact with MDM2 (Figure S8I). The asymmetric dimethylation on endogenous MDM2 was not detected upon Mina53 knockdown either (Figure S8J). Depletion of Mina53 increased the tetramerization of p53 compared with the scramble control in the absence of MDM2, suggesting that Mina53-mediated inhibition of p53 tetramerization is dependent on the me2a modification instead of MDM2-mediated p53 degradation (Figure S8K).

Last, we investigated whether Mina53-mediated regulation of p53 tetramerization, stability, and transcriptional activity affect chromatin modifications at p53 target gene promoters. The protein p300/CREB-binding protein catalyzes the acetylation of H3K14, H3K18, and H3K27 and serves as a key coactivator for p53-mediated transactivation.⁵⁰ ChIP assays revealed that Mina53 depletion significantly increased the acetylation of these histone residues at the *p21* promoter (Figure 5I). Consistently, ectopic expression of WT but not inactive mutant Mina53 suppressed acetylation of H3K14, H3K18, and H3K27 at the *p21* promoter (Figure 5J). Moreover, the effect of Mina53 on histone acetylation modifications was p53 dependent (Figure S8L).

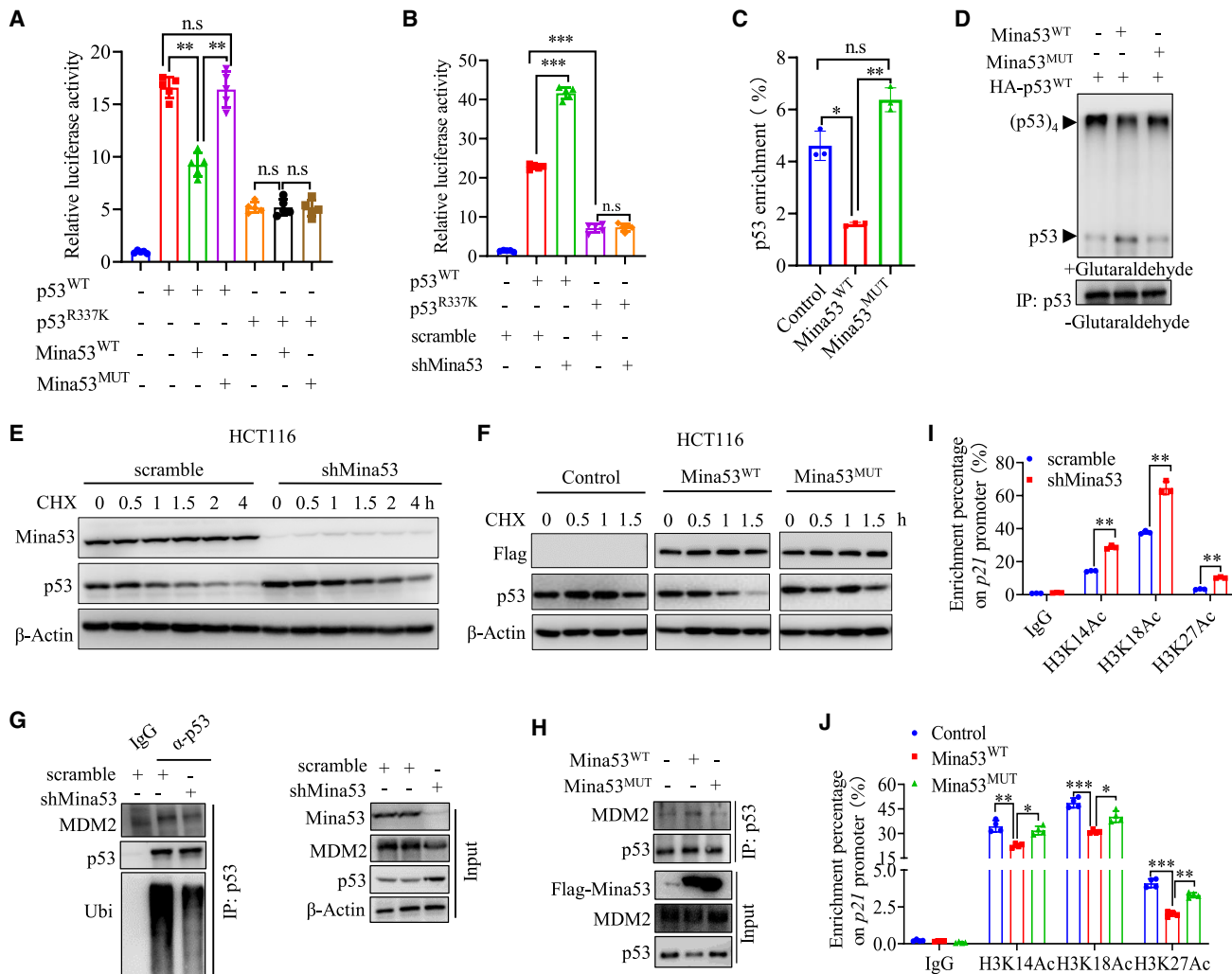


Figure 5. Mina53-mediated demethylation regulates p53 transcriptional activity, oligomerization, stability, and chromatin modifications

(A and B) Relative luciferase signals for the p21 promoter in HCT116 *p53*^{-/-} cells reconstituted with WT or R337K p53 and co-transfected with FLAG-tagged WT or inactive mutant Mina53 (A) or infected with lentiviruses containing scramble or Mina53 shRNA (B).

(C) The enrichment of p53 on the promoter of p21 in HCT116 cells ectopically expressing WT or inactive mutant Mina53.

(D) Immunoblot analysis of p53 oligomerization in HCT116 cells ectopically expressing WT or inactive mutant Mina53.

(E and F) Immunoblot analysis of endogenous p53 levels in HCT116 cells upon depletion of Mina53 (E) or ectopic expression of WT or inactive mutant Mina53 (F) in the presence of CHX at the indicated time points.

(G and H) Immunoblot analysis of the interaction between MDM2 and p53 in HCT116 cells infected with lentiviruses expressing scramble or Mina53 shRNA (G) or with ectopic expression of WT or inactive mutant Mina53 (H).

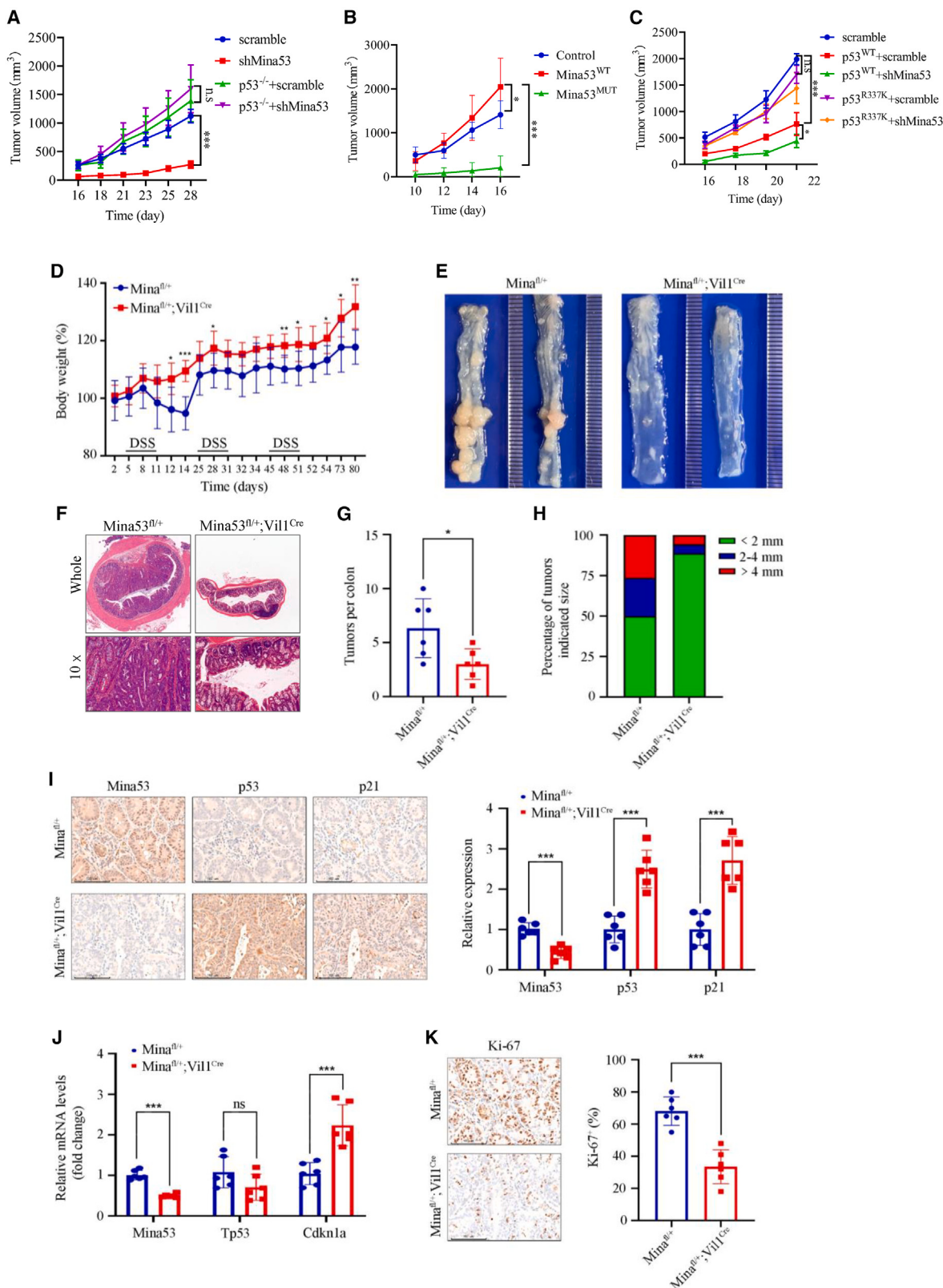
(I and J) ChIP analysis of p53-dependent histone acetylation at the *p21* promoter in HCT116 cells infected with lentiviruses expressing scramble or Mina53 shRNA (I) or in HCT116 cells with ectopic expression of WT or inactive mutant Mina53 (J).

Collectively, these data suggest that Mina53 represses p53 signaling by inhibiting p300-dependent acetylation on p53 target gene promoters.

Mina53-mediated p53 inhibition is important for tumor growth *in vitro* and *in vivo*

To explore the biological function of Mina53, we first performed cell proliferation analysis. Mina53 knockdown led to a significant reduction in cell proliferation in HCT116 and A549 cells

(Figure S9A). However, in HCT116 *p53*^{-/-} cells and H1299 cells (*p53* null), the growth inhibition caused by Mina53 knockdown was largely diminished (Figure S9B), indicating that Mina53 depletion represses cell proliferation in a *p53*-dependent manner. Forced expression of WT Mina53, but not the catalytically inactive mutant, accelerated cell proliferation of HCT116 cells (Figure S9C). In the cells with depletion of endogenous Mina53, reconstituted expression of WT but not the inactive mutant Mina53 rescued cell proliferation (Figure S9D). In



(legend on next page)

addition, ectopic expression of R337K p53 enhanced cell proliferation compared to WT p53 expression (Figure S9E). Depletion of Mina53 suppressed cell proliferation in cells expressing WT but not R337K p53 (Figure S9E). Consistent results were obtained with colony formation assays (Figure S9F). Together, these results demonstrate that Mina53-mediated demethylation of p53 promotes cell proliferation.

The effect of Mina53 on tumor growth was further investigated using xenograft models. Mina53 depletion significantly suppressed tumor growth of HCT116 cells, but the effect was diminished when HCT116 *p53*^{-/-} cells were used (Figures 6A and S9G). Reconstituted expression of WT but not inactive mutant Mina53 promoted tumor growth (Figures 6B and S9H). Moreover, re-expression of R337K p53 in HCT116 *p53*^{-/-} cells rescued the growth suppression induced by Mina53 knockdown as compared to re-expression of WT p53 (Figures 6C and S9I).

To further verify the tumorigenic role of Mina53 *in vivo*, *Mina53* heterozygous mice on a C57BL/6J background were generated by crossing *Mina53*^{flox/+} mice with *Vil-Cre* mice. The results indicated that genetic ablation of *Mina53* in the intestinal epithelium showed no phenotype changes in mice, including appearance, body weight, or intestine development (Figures S10A–S10C). Nevertheless, in the Azoxymethane (AOM)/Dextran Sodium Sulfate (DSS)-induced model of colorectal cancer, depletion of *Mina53* in intestinal epithelial cells remarkably improved the body weight during tumorigenesis (Figure 6D). After the sacrifice of mice, we found that *Mina53* knockout mice developed much fewer and smaller tumors in the colorectum (Figures 6E–6H). Immunohistochemistry analysis revealed increased protein expression of p53 and its target gene *p21* in *Mina53* heterozygous mice (Figure 6I). In addition, *Mina53* knockout upregulated the mRNA levels of *Cdkn1a* but not of *Tp53* (Figure 6J). Ki-67 staining also confirmed that knockout of *Mina53* repressed the proliferation of tumor cells (Figure 6K). Together, these results provide further evidence showing that Mina53 negatively regulates p53-mediated signaling to drive tumorigenesis. These results also highlight a possible mechanism for functional inactivation of p53 in human cancers.

To demonstrate the repressive effect of Mina53 on p53 under normal physiological conditions, we generated a lentivirus containing Mina53-targeting shRNA or the scramble shRNA and injected it into BALB/c mice via the portal vein. We anticipated that the lentivirus would accumulate in the liver, leading to the knockdown of Mina53 expression in the liver. Seven days after injection, the mice were sacrificed, and liver tissues were collected for immunoblotting and RT-PCR analysis. Encouragingly, liver tissues from mice injected with the *Mina53* shRNA lentivirus

showed a significant reduction in Mina53 expression, down to approximately 40% of that in the control group (Figure S10D). As expected, p53 and p21 expression was significantly increased. The RT-PCR results verified the reduction of *Mina53* expression. The mRNA levels of p21 were upregulated, while p53 mRNA levels remained unchanged (Figure S10E). Together, these results provide further evidence to support the notion that Mina53 negatively regulates p53-mediated signaling *in vivo*.

DISCUSSION

The tumor suppressor p53 is one of the most important guardians against unchecked cell growth. Studies have revealed an array of post-translational modifications present in p53 that contribute to its cellular homeostasis and activation upon stress, which include, but are not limited to, phosphorylation, acetylation, methylation, O-GlcNAcylation, and UFMylation, which regulate the stability, oligomerization, cellular localization, and transcription activity of p53.^{51–53} Here, we identify previously uncharacterized arginine asymmetric dimethylation on R337 of p53, which is crucial for p53 homeostasis. Importantly, the mutation R337H has been identified in different tumors, such as adrenocortical carcinoma, uterine epithelioid leiomyosarcoma, breast invasive ductal carcinoma, lung adenocarcinoma, and colorectal adenocarcinoma.^{54,55} This further illustrates the importance of p53R337me2a for the function of p53.

Our results demonstrate that Mina53 acts as a transcriptional co-repressor of p53 by catalyzing the removal of R337me2a modification on p53 to suppress p53 signaling (Figure S13F). In our study, we believe that Mina53 regulates p53 stability through the canonical mechanism dependent on MDM2. On the other hand, the oligomerization level of p53 increased upon Mina53 depletion, even in the absence of MDM2, suggesting that Mina53 regulates p53 oligomerization independent of MDM2. Thus, the finding that p53R337me2a is regulated by Mina53 adds a level of complexity to the regulation of p53 homeostasis and activity.

Arginine methylation has been demonstrated on many histone and non-histone substrates.^{56–59} However, the existence and the biological relevance of arginine demethylases are highly controversial. The identification and a full characterization of arginine demethylases is central to the concept that arginine methylation is a dynamic process in cells. Members of the JmjC family of 2OG-dependent oxygenases have been reported to possess arginine demethylation activity. Among them, JMJD6 was the first putative histone arginine demethylase but was later shown to be a lysine hydroxylase.^{60,61} Other members (KDM3A,

Figure 6. Mina53-mediated demethylation is important for tumor growth

- (A) Analysis of tumor growth rates of HCT116 cells and HCT116 *p53*^{-/-} cells infected with lentiviruses expressing scramble or Mina53 shRNA.
- (B) Analysis of tumor growth rates of HCT116 cells depleted of endogenous Mina53 and reconstituted with WT or the inactive mutant Mina53.
- (C) Analysis of tumor growth rates of HCT116 *p53*^{-/-} cells reconstituted with WT or R337K p53 and co-transfected with lentiviruses containing scramble or Mina53 shRNA.
- (D–K) *Mina53*^{flox/+} mice or *Mina53*^{flox/+;VilCre} mice were utilized in the AOM/DSS-induced colorectal cancer model ($n = 6$ in each group). Each mouse was weighed every 3 days after tumor induction (D). After sacrifice, colorectum tissues were collected (E and F). Tumor numbers (G) and sizes (H) were determined. Immunohistochemistry staining was performed to detect Mina53, p53, and p21 protein expression, and representative images are shown on the left (I). The mRNA expression levels of *Mina53*, *Tp53*, and *Cdkn1a* were analyzed (J). The proliferation marker Ki-67 in the tumor sections was also stained and analyzed (K). Error bars denote the mean \pm SD; $n = 6$ assays. Statistical analyses were performed by unpaired two-tailed Student's t test (* $p < 0.05$, ** $p < 0.01$, *** $p < 0.001$).

KDM4E, KDM5C, and JMJD1B) have been shown to possess both lysine demethylation and arginine demethylation activities on histone substrates.^{62,63} Our current study reveals that Mina53 is an arginine demethylase acting on a non-histone substrate, p53, which was demonstrated both *in vitro* and *in vivo*, besides its recently reported role in neural stem/progenitor cell identity via its demethylation activity on histone H4.⁶⁴ In addition, by analyzing the RNA sequencing (RNA-seq) data, we noticed the enrichment of inflammatory pathways (Figure S13G), indicating a cellular function of Mina53 beyond the canonical p53-mediated pathway, which would be intriguing to explore in a future study. Taken together, accumulating evidence lends strong support to the existence of *bona fide* arginine demethylation mechanisms in cells and lays a foundation for unraveling the functional significance of dynamic arginine methylation in biology.

Limitations of the study

This study identified an enzymatic activity of Mina53, which catalyzes demethylation on R337me2a of p53. The use of a pan small-molecule inhibitor for type I PRMTs gave rise to a cellular phenotype resembling that with Mina53 overexpression, which implies the presence of certain type I PRMTs for the generation of R337me2a. However, we have not conclusively identified the methyltransferase for generating R337me2a on p53. In addition, the use of Mina53-specific small-molecule inhibitors will complement the current genetic depletion study and will have more promise for translational applications. The demethylation activity of Mina53 toward p53 synthetic peptides is rather low in our experimental settings, implying a structural preference for Mina53. Obtaining the three-dimensional structure of the Mina53-peptide substrate complex will further strengthen the classification of Mina53 as a demethylase. Our study primarily focuses on WT p53 regulated by the arginine demethylase activity of Mina53. There are several key clinical mutant points on p53, and we did not investigate the effects of Mina53 on the mutant p53-mediated signaling pathway. In this context, it remains unclear whether Mina53 can catalyze the demethylation on p53 mutants. Furthermore, if Mina53 is capable of catalyzing the demethylation of p53 mutants, then the subsequent functional changes of the p53 mutants and their impact on tumors need to be investigated further.

RESOURCE AVAILABILITY

Lead contact

Requests for further information, resources, and reagents should be directed to and will be fulfilled by the lead contact, Wen Yi (wyi@zju.edu.cn).

Materials availability

All reagents are available upon request.

Data and code availability

- RNA-seq data produced in this article have been deposited in the GEO database and are publicly available as of the date of publication. The accession number can be found in the [key resources table](#).
- All original data used for statistics and bar graphs in this article have been deposited at Zenodo and are publicly available as of the date of publication. The Zenodo code can be found in the [key resources table](#).

- Any additional information required to reanalyze the data reported in this paper is available from the [lead contact](#) upon request.

ACKNOWLEDGMENTS

We would like to thank Drs. Bing Zhu, Jun Chen, Donglai Wang, Binghui Shen, and Li Zheng for critical reading of this manuscript. This work was supported by the National Key Research and Development Program of China (2024YFA1306302 to W.Y. and Y.R.), the National Natural Science Foundation of China (NSFC; grants 22325704, 32271331, and 92353303 to W.Y. and 82122051 and 82073245 to Y.R.), and the Fundamental Research Funds for the Central Universities (226-2024-00055 and K20220228).

AUTHOR CONTRIBUTIONS

W.Y. directed the project. L.Z. and W.Y. conceived the idea of the project. L.Z., C.Z., Y.R., and W.Y. planned the experiments. L.Z., L.Y., S.S., Q.Z., Y.W., B.L., M.L., Y.S., and B.Y. performed the experiments. L.Z., L.W., B.L., B.Y., R.Z., C.Z., and W.Y. analyzed the data. L.Z. and W.Y. wrote the paper with input from the other authors.

DECLARATION OF INTERESTS

The authors declare no competing interests.

STAR METHODS

Detailed methods are provided in the online version of this paper and include the following:

- KEY RESOURCES TABLE
- EXPERIMENTAL MODEL AND STUDY PARTICIPANT DETAILS
 - Cell lines
 - Mouse experiments
 - Tumor tissues
- METHOD DETAILS
 - Construction of expression vectors and stable cell lines
 - Immunoblotting analysis
 - Protein purification
 - Co-immunoprecipitation assays
 - *In vitro* protein binding assay
 - RNA-seq
 - Chromatin immunoprecipitation assay (ChIP)
 - Cell cycle and cell apoptosis assay
 - *In vitro* demethylation assay
 - Mass spectrometry analysis of *in vitro* demethylation
 - Molecular modeling, docking and molecular dynamics simulations
 - P53 oligomerization analysis
 - Protein cross-linking and mass spectrometry assay
 - Dual luciferase activity assay
 - Mapping the p53 methylation sites by mass spectrometry
 - Mina53 hydroxylation assays
 - p53 peptide treatment in HCT116 cells
 - Cell proliferation assay
- QUANTIFICATION AND STATISTICAL ANALYSIS

SUPPLEMENTAL INFORMATION

Supplemental information can be found online at <https://doi.org/10.1016/j.celrep.2025.115242>.

Received: May 7, 2024

Revised: November 20, 2024

Accepted: January 8, 2025

Published: January 25, 2025

REFERENCES

1. Bedford, M.T., and Clarke, S.G. (2009). Protein Arginine Methylation in Mammals: Who, What, and Why. *Mol. Cell* 33, 1–13. <https://doi.org/10.1016/j.molcel.2008.12.013>.
2. Yang, Y., and Bedford, M.T. (2013). Protein Arginine Methyltransferases and Cancer. *Nat. Rev. Cancer* 13, 37–50. <https://doi.org/10.1038/nrc3409>.
3. Blanc, R.S., and Richard, S. (2017). Arginine Methylation: The Coming of Age. *Mol. Cell* 65, 8–24. <https://doi.org/10.1016/j.molcel.2016.11.003>.
4. Guccione, E., and Richard, S. (2019). The Regulation, Functions and Clinical Relevance of Arginine Methylation. *Nat. Rev. Mol. Cell Biol.* 20, 642–657. <https://doi.org/10.1038/s41580-019-0155-x>.
5. Wu, Q., Schapira, M., Arrowsmith, C.H., and Barsyte-Lovejoy, D. (2021). Protein Arginine Methylation: From Enigmatic Functions to Therapeutic Targeting. *Nat. Rev. Drug Discov.* 20, 509–530. <https://doi.org/10.1038/s41573-021-00159-8>.
6. Le Romancer, M., Treilleux, I., Leconte, N., Robin-Lespinasse, Y., Sentis, S., Boucheikioua-Bouzaghou, K., Goddard, S., Gobert-Gosse, S., and Corbo, L. (2008). Regulation of Estrogen Rapid Signaling through Arginine Methylation by PRMT1. *Mol. Cell* 31, 212–221. <https://doi.org/10.1016/j.molcel.2008.05.025>.
7. Guo, Z., Zheng, L., Xu, H., Dai, H., Zhou, M., Pascua, M.R., Chen, Q.M., and Shen, B. (2010). Methylation of FEN1 Suppresses Nearby Phosphorylation and Facilitates PCNA Binding. *Nat. Chem. Biol.* 6, 766–773. <https://doi.org/10.1038/nchembio.422>.
8. Sims, R.J., 3rd, Rojas, L.A., Beck, D.B., Bonasio, R., Schüller, R., Drury, W.J., 3rd, Eick, D., and Reinberg, D. (2011). The C-terminal Domain of RNA Polymerase II is Modified by Site-Specific Methylation. *Science* 332, 99–103. <https://doi.org/10.1126/science.1202663>.
9. Wang, Y.P., Zhou, W., Wang, J., Huang, X., Zuo, Y., Wang, T.S., Gao, X., Xu, Y.Y., Zou, S.W., Liu, Y.B., et al. (2016). Arginine Methylation of MDH1 by CARM1 Inhibits Glutamine Metabolism and Suppresses Pancreatic Cancer. *Mol. Cell* 64, 673–687. <https://doi.org/10.1016/j.molcel.2016.09.028>.
10. Kruiswijk, F., Labuschagne, C.F., and Vousden, K.H. (2015). p53 in survival, death and metabolic health: a lifeguard with a licence to kill. *Nat. Rev. Mol. Cell Biol.* 16, 393–405. <https://doi.org/10.1038/nrm4007>.
11. Kastenhuber, E.R., and Lowe, S.W. (2017). Putting p53 in Context. *Cell* 170, 1062–1078. <https://doi.org/10.1016/j.cell.2017.08.028>.
12. Huang, J., Perez-Burgos, L., Placek, B.J., Sengupta, R., Richter, M., Dorsey, J.A., Kubicek, S., Opravil, S., Jenuwein, T., and Berger, S.L. (2006). Repression of p53 Activity by Smyd2-mediated Methylation. *Nature* 444, 629–632. <https://doi.org/10.1038/nature05287>.
13. Huang, J., Sengupta, R., Espejo, A.B., Lee, M.G., Dorsey, J.A., Richter, M., Opravil, S., Shiekhattar, R., Bedford, M.T., Jenuwein, T., and Berger, S.L. (2007). p53 is Regulated by the Lysine Demethylase LSD1. *Nature* 449, 105–108. <https://doi.org/10.1038/nature06092>.
14. Tang, Y., Zhao, W., Chen, Y., Zhao, Y., and Gu, W. (2008). Acetylation is Indispensable for P53 Activation. *Cell* 133, 612–626. <https://doi.org/10.1016/j.cell.2008.03.025>.
15. Yuan, J., Luo, K., Zhang, L., Cheville, J.C., and Lou, Z. (2010). USP10 Regulates p53 Localization and Stability by Deubiquitinating P53. *Cell* 140, 384–396. <https://doi.org/10.1016/j.cell.2009.12.032>.
16. Cui, D., Xiong, X., Shu, J., Dai, X., Sun, Y., and Zhao, Y. (2020). FBXW7 Confers Radiation Survival by Targeting p53 for Degradation. *Cell Rep.* 30, 497–509.e4. <https://doi.org/10.1016/j.celrep.2019.12.032>.
17. Sykes, S.M., Mellert, H.S., Holbert, M.A., Li, K., Marmorstein, R., Lane, W.S., and McMahon, S.B. (2006). Acetylation of the P53 DNA-binding Domain Regulates Apoptosis Induction. *Mol. Cell* 24, 841–851. <https://doi.org/10.1016/j.molcel.2006.11.026>.
18. Lee, J., Kim, D.H., Lee, S., Yang, Q.H., Lee, D.K., Lee, S.K., Roeder, R.G., and Lee, J.W. (2009). A Tumor Suppressive Coactivator Complex of P53 Containing ASC-2 and Histone H3-Lysine-4 Methyltransferase MLL3 or its Parologue MLL4. *Proc. Natl. Acad. Sci. USA* 106, 8513–8518. <https://doi.org/10.1073/pnas.0902873106>.
19. Wang, D., Kon, N., Lasso, G., Jiang, L., Leng, W., Zhu, W.G., Qin, J., Honig, B., and Gu, W. (2016). Acetylation-Regulated Interaction Between p53 and SET Reveals a Widespread Regulatory Mode. *Nature* 538, 118–122. <https://doi.org/10.1038/nature19759>.
20. Chuikov, S., Kurash, J.K., Wilson, J.R., Xiao, B., Justin, N., Ivanov, G.S., McKinney, K., Tempst, P., Prives, C., Gamblin, S.J., et al. (2004). Regulation of p53 Activity through Lysine Methylation. *Nature* 432, 353–360. <https://doi.org/10.1038/nature03117>.
21. Shi, X., Kachirskaia, I., Yamaguchi, H., West, L.E., Wen, H., Wang, E.W., Dutta, S., Appella, E., and Gozani, O. (2007). Modulation of p53 Function by SET8-mediated Methylation at Lysine 382. *Mol. Cell* 27, 636–646. <https://doi.org/10.1016/j.molcel.2007.07.012>.
22. Kurash, J.K., Lei, H., Shen, Q., Marston, W.L., Granda, B.W., Fan, H., Wall, D., Li, E., and Gaudet, F. (2008). Methylation of p53 by Set7/9 Mediates p53 Acetylation and Activity in Vivo. *Mol. Cell* 29, 392–400. <https://doi.org/10.1016/j.molcel.2007.12.025>.
23. Cui, G., Park, S., Badeaux, A.I., Kim, D., Lee, J., Thompson, J.R., Yan, F., Kaneko, S., Yuan, Z., Botuyan, M.V., et al. (2012). PHF20 is an Effector Protein of p53 Double Lysine Methylation that Stabilizes and Activates p53. *Nat. Struct. Mol. Biol.* 19, 916–924. <https://doi.org/10.1038/nsmb.2353>.
24. Berger, S.L. (2008). Out of the Jaws of Death: PRMT5 Steers P53. *Nat. Cell Biol.* 10, 1389–1390. <https://doi.org/10.1038/ncb1208-1389>.
25. Jansson, M., Durant, S.T., Cho, E.C., Sheahan, S., Edelmann, M., Kessler, B., and La Thangue, N.B. (2008). Arginine methylation regulates the p53 response. *Nat. Cell Biol.* 10, 1431–1439. <https://doi.org/10.1038/ncb1802>.
26. Lu, Y., Chang, Q., Zhang, Y., Beezhold, K., Rojanasakul, Y., Zhao, H., Castranova, V., Shi, X., and Chen, F. (2009). Lung Cancer-Associated JmJc Domain Protein Mdig Suppresses Formation of Tri-Methyl Lysine 9 of Histone H3. *Cell Cycle* 8, 2101–2109. <https://doi.org/10.4161/cc.8.13.8927>.
27. Ge, W., Wolf, A., Feng, T., Ho, C.H., Sekirnik, R., Zayer, A., Granatino, N., Cockman, M.E., Loenarz, C., Loik, N.D., et al. (2012). Oxygenase-catalyzed ribosome hydroxylation occurs in prokaryotes and humans. *Nat. Chem. Biol.* 8, 960–962. <https://doi.org/10.1038/nchembio.1093>.
28. Chowdhury, R., Sekirnik, R., Brissett, N.C., Krojer, T., Ho, C.H., Ng, S.S., Clifton, I.J., Ge, W., Kershaw, N.J., Fox, G.C., et al. (2014). Ribosomal oxygenases are structurally conserved from prokaryotes to humans. *Nature* 510, 422–426. <https://doi.org/10.1038/nature13263>.
29. Teye, K., Tsuneoka, M., Arima, N., Koda, Y., Nakamura, Y., Ueta, Y., Shirouzu, K., and Kimura, H. (2004). Increased Expression of a Myc Target Gene Mina53 in Human Colon Cancer. *Am. J. Pathol.* 164, 205–216. [https://doi.org/10.1016/S0002-9440\(10\)63111-2](https://doi.org/10.1016/S0002-9440(10)63111-2).
30. Ishizaki, H., Yano, H., Tsuneoka, M., Ogasawara, S., Akiba, J., Nishida, N., Kojiro, S., Fukahori, S., Moriya, F., Matsuoka, K., and Kojiro, M. (2007). Overexpression of the Myc Target Gene Mina53 in Advanced Renal Cell Carcinoma. *Pathol. Int.* 57, 672–680. <https://doi.org/10.1111/j.1440-1827.2007.02156.x>.
31. Komiya, K., Sueoka-Aragane, N., Sato, A., Hisatomi, T., Sakuragi, T., Mit-suoka, M., Sato, T., Hayashi, S., Izumi, H., Tsuneoka, M., and Sueoka, E. (2010). Expression of Mina53, a Novel c-Myc Target Gene, is a Favorable Prognostic Marker in Early Stage Lung Cancer. *Lung Cancer* 69, 232–238. <https://doi.org/10.1016/j.lungcan.2009.10.010>.
32. Zhou, L., Zhang, T., Zhu, Q., Zhang, P., Yu, L., Shen, B., Yi, W., Qiu, M., and Zhu, C. (2019). Mina53 Regulates the Differentiation and Proliferation of Leukemia Cells. *Hematol. Oncol.* 37, 513–515. <https://doi.org/10.1002/hon.2621>.
33. Bunz, F., Dutriaux, A., Lengauer, C., Waldman, T., Zhou, S., Brown, J.P., Sedivy, J.M., Kinzler, K.W., and Vogelstein, B. (1998). Requirement for P53 and P21 to Sustain G2 Arrest After DNA Damage. *Science* 282, 1497–1501. <https://doi.org/10.1126/science.282.5393.1497>.

34. Lakin, N.D., and Jackson, S.P. (1999). Regulation of P53 in Response to DNA Damage. *Oncogene* 18, 7644–7655. <https://doi.org/10.1038/sj.onc.1203015>.
35. Amano, T., Nakamizo, A., Mishra, S.K., Gumin, J., Shinojima, N., Sawaya, R., and Lang, F.F. (2009). Simultaneous Phosphorylation of P53 at Serine 15 and 20 Induces Apoptosis in Human Glioma Cells by Increasing Expression of Pro-Apoptotic Genes. *J. Neuro Oncol.* 92, 357–371. <https://doi.org/10.1007/s11060-009-9844-1>.
36. Gesser, B., Rasmussen, M.K., Raaby, L., Rosada, C., Johansen, C., Kjellerup, R.B., Kragballe, K., and Iversen, L. (2011). Dimethylfumarate Inhibits MIF-induced Proliferation of Keratinocytes by Inhibiting MSK1 and RSK1 Activation and by Inducing Nuclear p-c-Jun (S63) and P-P53 (S15) Expression. *Inflamm. Res.* 60, 643–653. <https://doi.org/10.1007/s00111-011-0316-7>.
37. Arakaki, R., Ishimaru, N., and Hayashi, Y. (2010). Immunotherapeutic Targets in Estrogen Deficiency-Dependent Sjögren's Syndrome-Related Manifestations. *Immunotherapy* 2, 339–346. <https://doi.org/10.2217/imt.10.18>.
38. Nicola, J.M.L. (2008). A Central Role for CK1 in Catalyzing Phosphorylation of the p53 Transactivation Domain at Serine 20 after HHV-6B Viral Infection. *J. Biol. Chem.* 283, 28563–28573. <https://doi.org/10.1074/jbc.M804433200>.
39. Shi, Y., Lan, F., Matson, C., Mulligan, P., Whetstine, J.R., Cole, P.A., Casero, R.A., and Shi, Y. (2004). Histone Demethylation Mediated by the Nuclear Amine Oxidase Homolog LSD1. *Cell* 119, 941–953. <https://doi.org/10.1016/j.cell.2004.12.012>.
40. Tsukada, Y.I., Fang, J., Erdjument-Bromage, H., Warren, M.E., Borchers, C.H., Tempst, P., and Zhang, Y. (2006). Histone Demethylation by a Family of JmjC Domain-Containing Proteins. *Nature* 439, 811–816. <https://doi.org/10.1038/nature04433>.
41. Li, S., Ali, S., Duan, X., Liu, S., Du, J., Liu, C., Dai, H., Zhou, M., Zhou, L., Yang, L., et al. (2018). JMJD1B Demethylates H4R3me2s and H3K9me2 to Facilitate Gene Expression for Development of Hematopoietic Stem and Progenitor Cells. *Cell Rep.* 23, 389–403. <https://doi.org/10.1016/j.celrep.2018.03.051>.
42. Eram, M.S., Shen, Y., Szewczyk, M., Wu, H., Senisterra, G., Li, F., Butler, K.V., Kaniskan, H.Ü., Speed, B.A., Dela Seña, C., et al. (2016). A Potent, Selective, and Cell-Active Inhibitor of Human Type I Protein Arginine Methyltransferases. *ACS Chem. Biol.* 11, 772–781. <https://doi.org/10.1021/acscchembio.5b00839>.
43. Zhu, Y., He, X., Lin, Y.C., Dong, H., Zhang, L., Chen, X., Wang, Z., Shen, Y., Li, M., Wang, H., et al. (2019). Targeting PRMT1-mediated FLT3 methylation disrupts maintenance of MLL-rearranged acute lymphoblastic leukemia. *Blood* 134, 1257–1268. <https://doi.org/10.1182/blood.2019002457>.
44. Park, J.H., Li, J., Starost, M.F., Liu, C., Zhuang, J., Chen, J., Achatz, M.I., Kang, J.G., Wang, P.Y., Savage, S.A., and Hwang, P.M. (2018). Mouse homolog of the human TP53 R337H mutation reveals its role in tumorigenesis. *Cancer Res.* 78, 5375–5383. <https://doi.org/10.1158/0008-5472.CAN-18-0016>.
45. Alinari, L., Mahasenan, K.V., Yan, F., Karkhanis, V., Chung, J.H., Smith, E.M., Quinon, C., Smith, P.L., Kim, L., Patton, J.T., et al. (2015). Selective Inhibition of Protein Arginine Methyltransferase 5 Blocks Initiation and Maintenance of B-cell Transformation. *Blood* 125, 2530–2543. <https://doi.org/10.1182/blood-2014-12-619783>.
46. Webb, L.M., Amici, S.A., Jablonski, K.A., Savardekar, H., Panfil, A.R., Li, L., Zhou, W., Peine, K., Karkhanis, V., Bachelder, E.M., et al. (2017). PRMT5-Selective Inhibitors Suppress Inflammatory T Cell Responses and Experimental Autoimmune Encephalomyelitis. *J. Immunol.* 198, 1439–1451. <https://doi.org/10.4049/jimmunol.1601702>.
47. Haupt, Y., Maya, R., Kazaz, A., and Oren, M. (1997). Mdm2 Promotes the Rapid Degradation of p53. *Nature* 387, 296–299. <https://doi.org/10.1038/387296a0>.
48. Argentini, M., Barboule, N., and Waslylyk, B. (2001). The Contribution of the Acidic Domain of MDM2 to P53 and MDM2 Stability. *Oncogene* 20, 1267–1275. <https://doi.org/10.1038/sj.onc.1204241>.
49. Gottlieb, T.M., Leal, J.F.M., Seger, R., Taya, Y., and Oren, M. (2002). Cross-Talk Between Akt, P53 and Mdm2: Possible Implications for the Regulation of Apoptosis. *Oncogene* 21, 1299–1303. <https://doi.org/10.1038/sj.onc.1205181>.
50. Jin, Q., Yu, L.R., Wang, L., Zhang, Z., Kasper, L.H., Lee, J.E., Wang, C., Brindle, P.K., Dent, S.Y.R., and Ge, K. (2011). Distinct Roles of GCN5/PCAF-mediated H3K9ac and CBP/p300-mediated H3K18/27ac in Nuclear Receptor Transactivation. *EMBO J.* 30, 249–262. <https://doi.org/10.1038/emboj.2010.318>.
51. Kruse, J.P., and Gu, W. (2009). Modes of P53 Regulation. *Cell* 137, 609–622. <https://doi.org/10.1016/j.cell.2009.04.050>.
52. Liu, Y., Tavana, O., and Gu, W. (2019). P53 Modifications: Exquisite Decorations of the Powerful Guardian. *J. Mol. Cell Biol.* 11, 564–577. <https://doi.org/10.1093/jmcb/mjz060>.
53. Liu, J., Guan, D., Dong, M., Yang, J., Wei, H., Liang, Q., Song, L., Xu, L., Bai, J., Liu, C., et al. (2020). UFMylation Maintains Tumour Suppressor P53 Stability by Antagonizing its Ubiquitination. *Nat. Cell Biol.* 22, 1056–1063. <https://doi.org/10.1038/s41556-020-0559-z>.
54. Pinto, E.M., and Zambetti, G.P. (2020). What 20 Years of Research Has Taught Us About the TP53p.R337H Mutation. *Cancer* 126, 4678–4686. <https://doi.org/10.1002/cncr.33143>.
55. Mathias, C., Bortolotto, S., Centa, A., Komechen, H., Lima, R.S., Fonseca, A.S., Sebastião, A.P., Urban, C.A., Soares, E.W.S., Prando, C., et al. (2020). Frequency of the TP53 R337H variant in sporadic breast cancer and its impact on genomic instability. *Sci. Rep.* 10, 16614. <https://doi.org/10.1038/s41598-020-73282-y>.
56. Hofweber, M., Hutten, S., Bourgeois, B., Spreitzer, E., Niedner-Boblenz, A., Schifferer, M., Ruepp, M.D., Simons, M., Niessing, D., Madl, T., and Dormann, D. (2018). Phase Separation of FUS is Suppressed by its Nuclear Import Receptor and Arginine Methylation. *Cell* 173, 706–719.e13. <https://doi.org/10.1016/j.cell.2018.03.004>.
57. Guccione, E., and Richard, S. (2019). The regulation, functions and clinical relevance of arginine methylation. *Nat. Rev. Mol. Cell Biol.* 20, 642–657. <https://doi.org/10.1038/s41580-019-0155-x>.
58. Xu, J., and Richard, S. (2021). Cellular Pathways Influenced by Protein Arginine Methylation: Implications for Cancer. *Mol. Cell* 87, 4357–4368. <https://doi.org/10.1016/j.molcel.2021.09.011>.
59. Yin, S., Liu, L., Brobbey, C., Palanisamy, V., Ball, L.E., Olsen, S.K., Ostrowski, M.C., and Gan, W. (2021). PRMT5-mediated Arginine Methylation Activates AKT Kinase to Govern Tumorigenesis. *Nat. Commun.* 12, 3444. <https://doi.org/10.1038/s41467-021-23833-2>.
60. Chang, B., Chen, Y., Zhao, Y., and Bruick, R.K. (2007). JMJD6 is a Histone Arginine Demethylase. *Science* 318, 444–447. <https://doi.org/10.1126/science.1145801>.
61. Webby, C.J., Wolf, A., Gromak, N., Dreger, M., Kramer, H., Kessler, B., Nielsen, M.L., Schmitz, C., Butler, D.S., Yates, J.R., 3rd., et al. (2009). Jmj6 Catalyses Lysyl-Hydroxylation of U2AF65, a Protein Associated with RNA Splicing. *Science* 325, 90–93. <https://doi.org/10.1126/science.11758>.
62. Walport, L.J., Hopkinson, R.J., Chowdhury, R., Schiller, R., Ge, W., Kawamura, A., and Schofield, C.J. (2016). Arginine Demethylation is Catalysed by a Subset of JmjC Histone Lysine Demethylases. *Nat. Commun.* 7, 11974. <https://doi.org/10.1038/ncomms11974>.
63. Tsai, W.C., Reineke, L.C., Jain, A., Jung, S.Y., and Lloyd, R.E. (2017). Histone Arginine Demethylase JMJD6 is Linked to Stress Granule Assembly through Demethylation of the Stress Granule-Nucleating Protein G3BP1. *J. Biol. Chem.* 292, 18886–18896. <https://doi.org/10.1074/jbc.M117.800706>.
64. Zhou, L., Zhao, X., Sun, J., Zou, K., Huang, X., Yu, L., Wu, M., Wang, Y., Li, X., and Yi, W. (2024). Mina53 demethylates histone H4 arginine 3

- asymmetric dimethylation to regulate neural stem/progenitor cell identity. *Nat. Commun.* 15, 10227. <https://doi.org/10.1038/s41467-024-54680-6>.
65. Emamzadah, S., Tropia, L., and Halazonetis, T.D. (2011). Crystal structure of a multidomain human p53 tetramer bound to the natural CDKN1A (p21) p53-response element. *Mol. Cancer Res.* 9, 1493–1499. <https://doi.org/10.1158/1541-7786.MCR-11-0351>.
66. Huang, J., Rauscher, S., Nawrocki, G., Ran, T., Feig, M., de Groot, B.L., Grubmüller, H., and MacKerell, A.D., Jr. (2017). CHARMM36m: an improved force field for folded and intrinsically disordered proteins. *Nat. Methods* 14, 71–73. <https://doi.org/10.1038/nmeth.4067>.
67. Chowdhury, R., Sekirnik, R., Brissett, N.C., Krojer, T., Ho, C.H., Ng, S.S., Clifton, I.J., Ge, W., Kershaw, N.J., Fox, G.C., et al. (2014). Ribosomal oxygenases are structurally conserved from prokaryotes to humans. *Nature* 510, 422–426. <https://doi.org/10.1038/nature13263>.
68. Eberhardt, J., Santos-Martins, D., Tillack, A.F., and Forli, S. (2021). Auto-Dock Vina 1.2.0: New Docking Methods, Expanded Force Field, and Python Bindings. *J. Chem. Inf. Model.* 61, 3891–3898. <https://doi.org/10.1021/acs.jcim.1c00203>.
69. Jumper, J., Evans, R., Pritzel, A., Green, T., Figurnov, M., Ronneberger, O., Tunyasuvunakool, K., Bates, R., Žídek, A., Potapenko, A., et al. (2021). Highly accurate protein structure prediction with AlphaFold. *Nature* 596, 583–589. <https://doi.org/10.1038/s41586-021-03819-2>.
70. Abraham, M.J., Murtola, T., Schulz, R., Páll, S., Smith, J.C., Hess, B., and Lindahl, E. (2015). GROMACS: High performance molecular simulations through multi-level parallelism from laptops to supercomputers. *SoftwareX* 1–2, 19–25. <https://doi.org/10.1016/j.softx.2015.06.001>.
71. Ledermann, D.W. (2018). [Sir Arthur Conan Doyle, Sherlock Holmes and infectious diseases]. *Nat. Rev. Chilena Infectol.* 114, 1267–1273. <https://doi.org/10.1016/j.bjpi.2018.01.033>.

STAR★METHODS

KEY RESOURCES TABLE

REAGENT or RESOURCE	SOURCE	IDENTIFIER
Antibodies		
Rabbit polyclonal anti-dimethyl-Arginine, asymmetric	Merck Millipore	Cat# 07–414; RRID:AB_310596
Rabbit monoclonal anti-p53(phosphor S15)	Abcam	Cat# ab223868; RRID: AB_2313773
Rabbit monoclonal anti-p53	Cell Signaling	Cat# 2527; RRID:AB_10695803
Mouse monoclonal anti-p53	Abcam	Cat# ab1101; RRID:AB_297667
Rabbit polyclonal anti-dimethyl-Arginine, symmetric	Merck Millipore	Cat# 07–412; RRID: AB_11212396
Anti-mono methyl Arginine	Abcam	Cat# ab414; RRID: AB_308709
Anti-Methylated Lysine	Abcam	Cat# ab23366; RRID: AB_447401
Rabbit monoclonal anti-MDM2	Abcam	Cat# ab259265; RRID: AB_2920616
Rabbit monoclonal anti-KDM2A	Abcam	Cat# ab191387; RRID: AB_2928955
Rabbit monoclonal anti-KDM3A	Abcam	Cat# ab191389; RRID: AB_2313773
Rabbit monoclonal anti-KDM4A	Abcam	Cat# ab191433; RRID: AB_2313773
Rabbit monoclonal anti-KDM5C	Abcam	Cat# ab194288; RRID: AB_2313773
Rabbit monoclonal anti-KDM6B	Abcam	Cat# ab169197; RRID: AB_2313773
Rabbit monoclonal anti-ROX2	Abcam	Cat# ab173573; RRID: AB_2313773
Rabbit monoclonal anti-FLAG	Abcam	Cat# ab236777; RRID: AB_2313773
Mouse monoclonal anti-FLAG	Sigma	Cat# F3165; RRID: AB_259529
Rabbit monoclonal anti-H3 (acetyl K14)	Abcam	Cat# ab52946; RRID: AB_880442
Rabbit monoclonal anti-H3(acetyl K18)	Abcam	Cat# ab40888; RRID: AB_732923
Rabbit monoclonal anti-H3	Abcam	Cat# ab1791; RRID: AB_302613
Rabbit monoclonal anti-H3(acetyl K27)	Abcam	Cat# ab177178; RRID: AB_732923
Rabbit monoclonal anti-p53R337me2a	This paper	N/A; RRID: AB_2313773
Rabbit monoclonal anti-HA	Cell Signaling	Cat# 3724; RRID: AB_1549585
Rabbit monoclonal anti-ubiquitin (E4I2J)	Cell Signaling	Cat# 43124; RRID: AB_2799235
HRP-labeled anti-β-Actin	Proteintech	Cat# HRP-60008; RRID: AB_2819183
Rabbit monoclonal anti-GST	Beyotime	Cat# AF2299; RRID: AB_2313773
Rabbit monoclonal anti-His	Beyotime	Cat# AF5056; RRID: AB_2313773
Chemicals, peptides, and recombinant proteins		
p53R337me2a peptide –1: RGRER (me2a) FEMFRELN EAL	This paper	N/A
p53R337me2a peptide –2: RGRER(m32a) FEMFR	This paper	N/A
p53R337me1 peptide: RGRER (me1) FEM FRELNEAL	This paper	N/A
p53R337me2a peptide –2: RGRER (me2s) FEMFR	This paper	N/A
p53R335me2s peptide: RGR (me2s) ERF EMFRELNEAL	This paper	N/A
p53R335me2a peptide: RGR (me2a) ERF EMFRELNEAL	This paper	N/A
p53R335me1 peptide: RGR (me1) ERFE MFRELNEAL	This paper	N/A
p53R333me2a peptide: R (me2a) GRER FEMFRELNEAL	This paper	N/A

(Continued on next page)

Continued

REAGENT or RESOURCE	SOURCE	IDENTIFIER
p53R333me2s peptide: R (me2s) GRER FEMFRELNEAL	This paper	N/A
p53R333me1 peptide: R (me1) GRER FEMFRELNEAL	This paper	N/A
p53Rme0 peptide -1: RGRERFEMFRELNEAL	This paper	N/A
p53Rme0 peptide-2: RGRERFEMFR	This paper	N/A
RNAiso Plus	Takara	Cat# 9108
Cycloheximide (CHX)	Cell signaling	Cat# 2112; CAS No. 66-81-9
Thymidine	Sigma	Cat# T1895; CAS No. 50-89-5
MG132	Sigma	Cat# M8699; CAS No. 133407-82-6
CMP-5	MCE	Cat# HY-120137; CAS No. 880813-42-3
DMSO	Sigma	Cat# D2650; CAS No. 67-68-5
Ascorbic Acid	Sigma	Cat# 255564; CAS No. 50-81-7
α -ketoglutarate	Sigma	Cat# 75890; CAS No. 328-50-7
Ammonium ferrous sulfate	Sigma	Cat#203505; CAS No. 7783-85-9
Ni-NTA Agarose	QIAGEN	Cat# 30210
Anti-Flag M2 magnetic beads	Sigma	Cat# 8823
Sep-Pak C18 1 cc Vac Cartridge	Waters	Cat# WAT023590
Magna ChIP Protein G Magnetic Beads	Millipore	Cat# 16-662
Protein A/G magnetic beads	MCE	Cat# HY-K0202
Anti-HA magnetic Beads	MCE	Cat# HY-K0201
Deposited data		
RNA-seq	Gene Expression Omnibus	GSE214730
Source data for statistics and bar graphs	Zenodo	14563467
Experimental models: Cell lines		
293T	ATCC	CRL-3216
HCT116	ATCC	CCL-247
A549	ATCC	CCL-185
MCF7	ATCC	HTB-22
H1299	ATCC	CRL-5803
HCT116 p53 ^{-/-}	A gift from Donglai Wang's Lab	N/A
Experimental models: Organisms/strains		
BALB/c Nude Mouse	The Jackson Laboratory	JAX™ No: 000711
C57BL/6JCya-Riox2 ^{em1flox} /Cya	Cyagen	S-CKO-13448
C57BL/6J Vil1 Cre	The Jackson Laboratory	RRID:IMSR_JAX:021504
Oligonucleotides		
Primers used in this article, see Table S4	This paper	N/A
Software and algorithms		
GraphPad Prism 8	GraphPad	https://www.graphpad.com/
Alphafold 2	Google	https://github.com/google-deepmind/alphafold
ImageJ	National Institutes of Health	https://imagej.net/ij/
Xcalibur	Thermo Fisher	https://www.thermofisher.cn/cn/zh/home/industrial/mass-spectrometry/liquid-chromatography-mass-spectrometry-lc-ms/lc-ms-software/lc-ms-data-acquisition-software/xcalibur-data-acquisition-interpretation-software.html
FlowJo	BD	https://www.flowjo.com/solutions/flowjo

EXPERIMENTAL MODEL AND STUDY PARTICIPANT DETAILS

Cell lines

Cell lines 293T, HCT116, A549, MCF7 and H1299 were all obtained from American Type Cell Culture (ATCC). HCT116 *p53*^{-/-} cell line is a gift from Donglai Wang's Lab. Cell lines were cultured in Dulbecco's Modified Eagle Medium (DMEM) medium (Hyclone), supplemented with 10% fetal calf serum (Gibco), 100 U/mL penicillin, and 100 U/mL streptomycin, in a humidified cell incubator at 37°C with an atmosphere of 5% CO₂. Cell lines used in this article have been validated by STR. As for cell lines overexpressing Mina53, cells were detected by Western blotting and real-time PCR to determine the expression level of Mina53 before each use. As for HCT116 *p53*^{-/-} cells, cells were detected by Western blotting using the anti-p53 antibody. Cell lines were tested for mycoplasma contamination with the MycAway Plus-Color One-Step Mycoplasma Detection Kit and were confirmed negative.

Mouse experiments

All animal studies were carried out in the Laboratory Animal Centers of Zhejiang University and Fudan University, and the protocols were approved by the Research Ethic Committees of Zhejiang University and Fudan University, respectively.

AOM/DSS-induced colorectal cancer model: *Mina53*^{flox/+} mice were generated by co-injecting the gRNA targeting *Mina53* gene, the donor vector containing *loxP* sites, and Cas9 mRNA into fertilized mouse eggs to generate targeted conditional knockout offspring. F0 founder animals were identified by PCR followed by sequence analysis, which were bred to wildtype mice to test germ-line transmission and F1 animal generation. The generated *Mina53*^{flox/+} mice were housed in a specific pathogen-free room. Heterozygous *Mina53* conditional knock-out mice on a C57BL/6J background were generated by crossing *Mina53*^{flox/+} mice with Cre recombinase transgenic mice driven by the *Villin* promoter (See [Table S4](#) for primers used for genotyping). Male and female mice at the age of six weeks were subjected to AOM/DSS induction. Mice were injected intraperitoneally with 10 mg of azoxymethane per kg body weight. After 5 days, 2% DSS was given in the drinking water for 6 days followed by regular drinking water for 2 weeks. This cycle was repeated twice more with 1.5% DSS and mice were killed on day 80. Colorectal tumor tissues were collected and applied to further analysis. This study was performed in Fudan University.

Xenograft study: 5×10⁶ HCT116 cells (stably expressing Mina53 shRNA or scramble shRNA) or HCT116 *p53*^{-/-} cells (stably expressing Mina53 shRNA, scramble shRNA, rescued with re-expressing p53^{WT}, or p53^{R337K}) were mixed with Matrigel (Corning) in a 1:1 ratio. The cell-matrix complex was subcutaneously injected into the flanks of 6-week-old male nude BALB/c mice. Tumor growth was monitored every 3 days over a 4-week period. At the end of the seventh week, the tumors were harvested and weighed. None of the experiments were exceeded the limit for tumor burden (10% of total bodyweight or 2 cm in diameter). This study was performed in Zhejiang University.

Targeted knockdown of Mina53 in the mouse liver: Scramble shRNA or Mina53 shRNA oligos were cloned into the pLKO.1-GFP lentiviral vector. The lentivirus was produced by co-transfected pLKO.1, pMD2.G and psPAX2 into HEK293T cells. 100 μL concentrated lentivirus with a titer of 5x10⁸ TU/mL were injected into the portal vein of each 6-week-old male BALB/c mouse using insulin needles. All surgical procedures were performed with the animals anesthetized by subcutaneous injection of 0.4 μg/kg chloral hydrate. After the surgery, animals were allowed to recover on a warming pad and then put back to the cage. After one week, mice were sacrificed. The livers of the mice were removed and observed by fluorescence microscope immediately. The tissues with high fluorescence signals were harvested, and equally divided into two portions for immunoblotting analysis and RT-PCR analysis, respectively. This study was performed in Zhejiang University.

Tumor tissues

Colon tumor tissues and matched adjacent peritumoral tissues from the same patient were obtained from the Bio-specimen Repository of the First Affiliated Hospital of Zhejiang University (Hangzhou, China). All patients were registered at the hospital and the informed consent was obtained from each patient before the study. These specimens were examined and diagnosed by pathologists at the First Affiliated Hospital. The research protocol was approved by the Ethic Committee of the School of Medicine, Zhejiang University (Hangzhou, China). The entire experimental protocol was conducted in compliance with the institutional guidelines. As to investigate the relationship between Mina53 and p53-target genes, we performed DNA-sequencing to screen tumors expressing wild-type p53 and 50 pairs of tumor samples with wild-type p53 expression were collected, and corresponding clinical pathological information of patients were provided in [Table S1](#). As for investigating Mina53 expression status in the tumor tissues and adjacent tissues, we collected 58 pairs of tumor samples, and the clinical pathological information of patients were provided in [Table S2](#).

METHOD DETAILS

Construction of expression vectors and stable cell lines

Human Mina53 cDNA or p53 cDNA (cDNA clones obtained from Origene) was cloned into different expression vectors in order to produce various fusion proteins using one step cloning kit: PCMV-N-Flag or pchN2-N-Flag for flag-tagged fusion proteins; PCMV-C-HA and pLVX-N-HA for HA-tagged fusion proteins; pet28a for His-tagged proteins and pGEX-4T1 for GST-tagged fusion proteins. The shRNA sequence targeting Mina53 (designed using the GPP Web Portal) or the corresponding scramble sequence was inserted into the lentiviral vector pLKO.1 to allow for the depletion of the endogenous Mina53.

To generate the point-mutation constructs, the plasmid containing the wild-type Mina53 cDNA or p53 cDNA was used as template and PCR was performed using primers with relative mutations. The PCR product was digested using Dpn1 and then transformed into the competent cell. The construct was further sequenced to confirm the sequence of the mutant plasmid.

To make HA-Mina53-stable cells, lentiviral stocks were generated in HEK293T cells with a three-plasmid packing system and used to infect HCT116 cells. After 48 h of infection, HCT116 cells were selected with puromycin (2 mg/mL) for one week and the concentration of puromycin was maintained at a concentration of 1 mg/mL during the lateral culturing.

Immunoblotting analysis

Cells were lysed in RIPA lysis buffer supplemented with complete protease inhibitors (Roche), and the lysate was resolved on 8–12% SDS-PAGE gel, transferred to nitrocellulose membrane, and immunoblotted with the indicated antibodies.

Protein purification

Flag-tagged Mina53 or p53 constructs were transfected into 293T cells for expression for 48 h. Cells were then collected and lysed in HEPES-KOH lysis buffer (50 mM Hepes-KOH, 150 mM NaCl, 2 mM EDTA, 1% Triton X-100 and protease inhibitor cocktail, PH 7.6). The lysates were further incubated with anti-Flag M2 magnetic beads at 4°C for 8 h. After washed three times with HEPES-KOH lysis buffer and three times with PBS buffer, the Flag-tagged Mina53 was eluted with PBS containing 3X Flag peptides.

The constructs for His-tagged Mina53, GST-tagged Mina53, and His-tagged p53 were expressed and purified in *E. coli* BL21. Briefly, the transformant were grown in LB at 37°C until the OD₆₀₀ of the culture was up to 0.6–0.8. Protein expression was induced at 25°C by addition of 1 mM of IPTG for 8 h. After lysis, the recombinant protein was purified by His-tag purification resin (Beyotime) or GST-tag purification resin (Beyotime) according to the manufacturer's protocol. The bound protein was eluted with the elution buffer (50 mM Tris, 150 mM NaCl, 50 mM imidazole for His-tag purification and 50 mM HEPES, 150 mM NaCl, 2 mM DTT and 5mM reduced glutathione for GST-tag purification) and concentrated by ultrafiltration.

Co-immunoprecipitation assays

As for the detection of endogenous interaction of Mina53 and p53, HCT116 cells or A549 cells were collected and lysed in the co-immunoprecipitation lysis buffer (40 mM HEPES-KOH, 85 mM NaCl, 0.1% NP40 and protease inhibitor cocktail, PH 7.6). After centrifugation, the supernatant was collected and incubated with protein A/G magnetic beads (MCE) and 1 μL Mina53 antibody or p53 antibody at 4°C overnight. Then the protein A/G beads were washed three times with the co-immunoprecipitation lysis buffer and the bound proteins were eluted using 0.2 M glycine-HCl buffer (PH 3.5). The proteins were further analyzed by immunoblotting with indicated antibodies.

As for detection of exogenous interactions of related proteins, the relative plasmids with FLAG tag or HA tag were transfected into 293T cells. Then 293T cells were collected and lysed in the co-immunoprecipitation lysis buffer. After centrifugation, the supernatant was incubated with an-flag magnetic M2 beads (Sigma) or anti-HA magnetic beads (MCE) 4°C overnight. Then beads were washed three times with the co-immunoprecipitation lysis buffer and the complex of proteins were eluted using flag peptide or HA peptide. Then the elution buffer was detected by immunoblotting with indicated antibodies.

In vitro protein binding assay

Equal amounts of bacterially purified His-tagged p53 and GST-tagged Mina53 were incubated with GST-Sepharose beads in the binding buffer (50 mM HEPES-KOH, 85 mM KCl, 2 mM EDTA and 0.5% NP-40, 1 x protease inhibitor cocktail) for 8 h at 4°C. After washing three times with binding buffer, the bound proteins were eluted by 1 x loading buffer (50 mM Tris-HCl, 2% SDS, 0.1% bromophenol blue, 10% glycerol, 1% β-mercaptoethanol, pH 6.8) and further analyzed by immunoblotting.

RNA-seq

HCT116 cells stably transfected with scramble shRNA or Mina53 shRNA were collected and the RNA of each sample was extracted by TRIzol (Invitrogen). The RNA-seq analysis was performed at National Healthcare Big Data (Eastern) Center (Nanjing, China). The mRNAs were enriched by poly-T attached magnetic beads and the libraries were then prepared. The qualified libraries were then sequenced using Illumina platform with PE150 sequencing strategy. After the clean reads were accessed, the sequences achieved were compared with the referenced genome and then mapped to the genome using HISAT2. As to quantify the expression level of a specific gene in RNA-seq analysis, the FPKM (fragments per kilobase per million mapped fragments) was introduced to represent the expression level of each gene and used to compare the differentially expressed genes. To retrieve potential p53 target genes which were repressed by Mina53 in a p53-dependent manner, we searched the filtered RNA-seq results using the following strategies: the expression level in the p53^{+/+}/shMina53 group was at least 1.5-fold higher than that in the p53^{+/+}/scramble shRNA group; the expression level in the p53^{+/+}/shMina53 group was at least 2-fold higher than that in the p53^{-/-}/shMina53 group. The filtered genes which were also verified as p53 target genes from the RNA-seq analysis were collected and presented as a heatmap. The RNA-seq data has been deposited in the GEO database with the accession number GSE214730.

Chromatin immunoprecipitation assay (ChIP)

Cells were fixed with 1% formaldehyde for 10 min at room temperature and the reaction was stopped by 0.125 M glycine. Then cells were lysed with 1 mL cell pre-lysis buffer (10 mM Tris-HCl, 25 mM KCl and 5 mM MgCl₂, pH7.4), and were centrifuged to extract the nuclei. The collected nuclei were lysed using 200 μ L nuclei lysis buffer (50 mM Tris-HCl, 10 mM EDTA and 1% SDS, pH8.0), and were sonicated using an ultrasonic cell disruptor (BRANSON SLPe Model). After centrifugation, the supernatant was incubated with protein A/G magnetic beads which had been washed three times using dilution buffer (16.7 mM Tris-HCl, 167 mM NaCl, 1.2 mM EDTA, 1.1% Triton X-100 and 0.01% SDS, pH 8.0). After wash the beads with low salt wash buffer (20 mM Tris-HCl, 150 mM NaCl, 2 mM EDTA, 1% Triton X-100 and 0.1% SDS, pH8.0), high salt wash buffer (20 mM Tris-HCl, 500 mM NaCl, 2 mM EDTA, 1% Triton X-100 and 0.1% SDS, pH 8.0), LiCl wash buffer (10 mM Tris-HCl, 0.25 M LiCl, 1% NP-40 and 1% deoxycholic acid, pH 8.0) and TE buffer, the DNA was eluted with 300 μ L of elution buffer (Tris-HCl 20 mM pH 7.5, 20 mM EDTA, 0.5% SDS, 500 μ g/mL Proteinase K) and incubated for 4 h at 56°C. The DNA was extracted with phenol-chloroform followed by purification using a Qiagen MinElute column. Quantitative PCR was performed to analyze the enrichment of corresponding genes (Table S4).

Cell cycle and cell apoptosis assay

For the cell cycle analysis, the cells were arrested by thymidine and then released from the G1 phase to indicated time points. The cells were washed three times with ice-cold PBS, and then fixed in 70% ethanol in PBS at 4°C for 12 h. After fixation, cells were washed with cold PBS and stained with 0.5 mL of propidium iodide (PI) staining buffer, which contains 200 mg/mL RNase A, 50 μ g/mL PI, at 37°C for 30 min in the dark. Analyses were performed on a CytoFLEX LX flow cytometer.

To assay cell apoptosis, the cells were treated with doxorubicin for 48 h, and the cell apoptosis analysis was performed using the Annexin V-FITC Apoptosis Detection Kit (Beyotime) according to the manufacturer's instruction. Early apoptotic cells were defined as Annexin-V-position, PI-negative cells. Analyses were performed on a CytoFLEX LX flow cytometer.

In vitro demethylation assay

Purified His-tagged Mina53 (2 μ g) was incubated with 1 μ g of the synthetic p53R337me2a peptide (RGRER(me2a)FEMFRELNEAL) in 50 μ L reaction buffer (50 mM HEPES-KOH, 150 mM NaCl, 1 mM α -ketoglutarate, 2 mM ascorbic acid, 150 mM ammonium ferrous sulfate and protease inhibitor cocktail) at 37°C for 1 h. The reaction activity was detected by dot blotting with the p53R337me2a site-specific antibody or a pan-antibody against asymmetric arginine di-methylation.

Another assay was carried out to examine the removal and conversion of the methyl group to formaldehyde during the reaction. In this assay, the enzyme activity was analyzed by the Hantzsch reaction using AAPT (acetoacet-p-toluidide), a modified NASH method. The reaction was quenched at indicated time points. After TCA (trichloroacetic acid) precipitation and the addition of 1% Tris buffer, an equal volume of AAPT buffer was added into the supernatant and the mixtures were incubated at room temperature for 30 min and further detected using a PHERAstar FS (BMG Labtech) plate reader with 355 nm excitation and 470 nm emission. The enzymatic kinetics parameters K_m, V_{max} and K_{cat} values were calculated according the reading.

Mass spectrometry analysis of in vitro demethylation

The demethylation reaction mixture was desalted by passing through a C18 ZipTip (Waters). The C18 ZipTips were activated using 80% acetonitrile with 0.1% TFA (trifluoroacetic acid), then equilibrated using 0.1% TFA. TFA and acetonitrile were separated added to the mixture to a final concentration of 0.2% and 2% and then the reaction mixture was loaded onto the activated C18 ZipTips. The C18 ZipTips were washed with 0.1% for three times and the bound peptides was eluted from the C18 ZipTips using 30% acetonitrile. After lyophilization, the eluted peptide was detected by high-resolution mass spectrometer (Thermo Fisher Scientific) at the First Affiliated Hospital of School of Medicine, Zhejiang University.

Molecular modeling, docking and molecular dynamics simulations

The initial model of the p53 tetramer was built based on the crystal structure of p53 tetramer (PDB ID 3TS8).⁶⁵ Arg337 residues were modeled as asymmetric dimethylarginines. The asymmetrically dimethylated p53 tetramer was subsequently placed into a periodic cubic box with sides of 11.9 nm solvated with ~53000 TIP3P water molecules containing Na⁺ and Cl⁻ ions at 0.15 M, resulting in ~174,000 atoms in total. The CHARMM36m force field⁶⁶ was used for the simulations. The system was energy minimized and equilibrated in a stepwise manner using 1 ns NVT simulations. And a following NPT simulation was further performed for 1 ns. Finally, a 500 ns production simulation was performed. In the productive simulation, the temperature was kept constant at 300 K using the v-rescale thermostat. Neighbor searching was performed every 5 steps. Neighbor searching was performed every 5 steps. The PME algorithm was used for electrostatic interactions. with a cut-off of 1 nm. A reciprocal grid of 80 × 80 × 80 cells was used with 4th order B-spline interpolation. A single cut-off of 1 nm was used for van der Waals interactions. The hydrogen mass repartitioning technique was employed with a single LINCS iteration (expansion order 4), allowing simulations to be performed with an integration time step of 4 fs.

The Mina53-p53 peptide complex was prepared by docking a p53 peptide with an asymmetrically di-methylated Arg (R_{me2a}) in the mid (RGRER_{me2a}FEMFR) to the crystal structure of Mina53 (PDB ID: 4BXF)⁶⁷ using AutoDock Vina.⁶⁸ The missing residues were modeled based on the AlphaFold2 predicted structure.⁶⁹ The Mn (II) and 2-oxoglutarate (2OG) substrates were kept in the pocket. The complex was then placed into a periodic cubic box with sides of 9.7 nm solvated with ~29,000 TIP3P water molecules containing

Na⁺ and Cl-ions at 0.15 M, resulting in ~93,000 atoms in total. The same force field parameters and simulation protocols were used for the complex, except otherwise specified.

A 500 ns MD simulation was performed to check the docked structure. We observed that the conformation of the p53 peptide was adjusted substantially in the complex, suggesting the docked conformation obtained from AutoDock Vina was not optimal. We then resorted to a 250 ns restrained MD by adding a harmonic potential to keep the sidechain of p53 R_{me2a} in the binding site but allowing other residues of the p53 peptide freely explore the conformational space. By doing so, we obtained an MD-optimized structure of the p53 peptide-Min53 complex which was finally shown to be very stable in a 1000 ns unbiased MD simulation. And the final frame of the simulation was used to analyze the interactions between p53 R337me2a and Min53.

All MD simulations were performed using Gromacs 2020.6.⁷⁰ The interactions were analyzed based on the last 100 ns by GetContacts scripts (<https://getcontacts.github.io/>) and CONAN.⁷¹ The figures were generated using PyMol software (The PyMOL Molecular Graphics System, Version 2.5 Schrödinger, LLC.).

P53 oligomerization analysis

293T cells transfected with flag-tagged p53^{WT}, p53^{R333K}, p53^{R335K}, P53^{R337K} or p53^{2RK} were lysed in cell lysis buffer (50 mM HEPES-KOH, 150 mM NaCl and 1% NP-40, pH 7.6). After ultrasonication, the glutaraldehyde was added into the cell lysate to a final concentration of 0.025%, and the reaction was allowed to proceed at room temperature for 15 min. The proteins were separated by SDS-PAGE, and further immunoblotted with anti-flag antibodies.

To detect the tetramerization of p53 regulated by Min53, HCT116 cells were infected with lentivirus containing the Min53 shRNA or the scramble shRNA and then collected 72 h later. The tetramerization of endogenous p53 was detected by immunoblotting using anti-p53 antibody.

Protein cross-linking and mass spectrometry assay

For protein cross-linking, Flag-tagged p53 was immunoprecipitated in M2 beads, and incubated with purified His-tagged Min53 in the buffer containing 50 mM HEPES pH 7.5 and 150 mM NaCl. The crosslinking reagent bis(sulfosuccinimidyl)suberate (BS3) was added to the buffer in a final concentration of 1 mM, and the reaction was allowed to proceed at room temperature for 1 h. The reaction was quenched by the addition of 50 mM ammonium bicarbonate. Then, the cross-linked beads were rinsed with PBS for 5 times to remove the excess of cross-linking solution. The denaturation buffer (40 µL 8 M urea, 100 mM Tris pH 8.5) was added to beads and rotated for 2 h. After denaturation, the sample was treated with 5 mM TCEP and 10 mM iodoacetamide for 20 min in the dark, and further digested in 2 M urea by trypsin/LysC Mix (at 50:1 protein: enzyme ratio) at 37°C for 16 h. Digestion was quenched by adding formic acid (5%, final concentration), and the digested peptides were desalted with StageTips and subjected to mass spectrometry analysis.

BS3 cross-linked peptides were identified using pLink 2 software. pLink 2 search parameters: precursor mass tolerance 20 parts per million (ppm), fragment mass tolerance 20 ppm, peptide length minimum 6 amino acids and maximum 60 amino acids per chain, peptide mass minimum 600 and maximum 6,000 Da per chain, variable modification Cys 57.02146, enzyme trypsin, three missed cleavage sites per chain.

Dual luciferase activity assay

The promoter of p21 containing the p53 binding site was cloned into the PGL3 vector using the whole genome DNA of HCT116 cells as template. HCT116 p53^{-/-} cells were seeded in 96-well plates and transfected with 500 ng of experimental plasmids (pGL3 basic vector, or PGL3 vector containing the p21 promoter with the PCMV empty vector, pCMV-p53^{WT} or PCMV-p53^{R337K} vector) and 25 ng of the TK-Renilla expression plasmid. Then 36 h after transfection, relative luciferase activity was determined using the Dual Luciferase Assay Kit (Beyotime) according to the manufacturer's protocol. In brief, the transfected cells were lysed using lysis buffer special for reporter gene containing cells and 100 µL firefly luciferase detection agent was added to each well. Then the RLU1 (relative light unit) was detected using the luminometer. Next, 100 µL mixture of renilla luciferase and coelenterazine was added and the RLU2 was also detected. The activation of the p21 promoter was determined as the value of RLU1/RLU2. The luciferase activity of the empty control group was determined as 1 and the relative luciferase activity of other group was a ratio compared with the empty control.

Mapping the p53 methylation sites by mass spectrometry

HCT116 cells were pretreated with Dox for 6 h to maximize the methylation levels. Then cells were collected and lysed in ice-cold cell lysis buffer (50 mM HEPES, 150 mM NaCl, 2 mM EDTA, 1% Triton X-100 and protein inhibitor cocktail, PH 7.6) and further subjected to immunoprecipitation with anti-p53 antibodies. The eluted p53 protein was added with urea to a final concentration of 6 M, and the sample was treated with 5 mM TCEP for 15 min followed by iodoacetamide for 20 min. Next, the dilution buffer (100 mM HEPES, 10 mM CaCl, pH 7.5) was added to the sample to make sure that the concentration of urea was less than 1 mM. Then the diluted samples were digested by chymotrypsin for 18 h at 25°C. The digested p53 protein was desalted using C18 Zip-tip (Millipore) and then detected by mass spectrum. The brief process of desalting was as follows: the Zip-tip was activated using 80% CAN/0.1% TFA and balanced by 0.1% TFA. Acidulating peptides mixture in 0.1% TFA was absorbed to the Zip-tip followed by desalting

the mixture twice using 0.1% TFA. Then the peptides mixture was eluted from the C18 Zip-tip using 50% CAN/0.1% TFA. After freeze drying, the peptide mixture was subjected to mass spectrometry analysis.

Mass spectrometry was carried out on an Orbitrap Fusion mass spectrometer (Thermo Fisher), which was operated in the positive-ion mode at an ion transfer tube temperature of 320°C. The positive-ion spray voltage was 2.0 kV. The Orbitrap Fusion Lumos was set to the OT-IT mode. For a full mass spectrometry survey scan, the target value was 5×10^5 and the scan ranged from 300 to 1,400 m/z at a resolution of 120,000 and a maximum injection time of 50 ms. For the MS2 scan, a duty cycle of 3 s was set with the top-speed mode. Only spectra with a charge state of 2–6 were selected for fragmentation by higher-energy collision dissociation with a normalized collision energy of 35%. The MS² spectra were acquired in the ion trap in rapid mode with an AGC target of 7,000 and a maximum injection time of 35 ms, and the dynamic exclusion was set to 18 s. The MS/MS spectra were searched against the Human UniProt FASTA database (UP000005640, containing 77027 entries) and Trypsin and Chymotrypsin were respectively selected as the digestive enzyme with two potential missed cleavages. Arginine methylation and di-methylation was set as variable modifications. The false discovery rate (FDR) for peptides and proteins was controlled <1% by Andromeda search engine. The MS quantitative data was analyzed via software MaxQuant (<http://maxquant.org/>, version 1.6.5.0).

Mina53 hydroxylation assays

Flag-tagged full-length Mina53 (Mina53^{WT}) protein or N terminus truncated Mina53 (Mina53^{Δ1–23}) protein was purified from 293T cells. Purified enzymes were incubated with the RPL27A peptide (RGNAGGLHHHRINFDKYHP) in the hydroxylation reaction buffer (50 mM Hepes-KOH, 150 mM NaCl, 2 mM ascorbate, 1 mM ZOG and 500 μM Fe (II), pH 7.5) at a mass ratio of 1:50. The reaction mixture was incubated at 37°C for 2 h and quenched with 0.1 μL TFA. After desalinating the mixture by C18 column, the elution was freeze-dried and re-dissolved using 50% methyl alcohol. Then the solution was injected into the ESI Mass spectrometer and the molecular weight was detected by MS.

p53 peptide treatment in HCT116 cells

Synthetic p53 peptides with cell penetrating peptide and FITC (CPP-p53R337me2a peptide or CPP-p53R337me0 peptide) were individually incubated with HCT116 cells at the concentration of 20 μM for 24 h. After cell lysis, the p53R337me2a levels and mRNA levels of p53-targeted genes, including *p21*, *FAS* and *NOX* were analyzed as stated above.

Cell proliferation assay

Approximately 1×10^3 cells were seeded into 96-well plates with three replicates. Cell proliferation was monitored by using the enhanced cell counting kit-8 according to the manufacturer's protocol (Beyotime).

QUANTIFICATION AND STATISTICAL ANALYSIS

Data are presented as the means ± standard deviations (S.D.). Statistical analyses were performed by unpaired two-tailed Student's t-tests using GraphPad Prism 8. Data were derived from at least three independent biological replicate experiments and are presented as the mean ± S.D; a value of $p < 0.05$ was considered statistically significant. All statistics details can be found in the relative figure legends.